First Excursion Probability Sensitivity in Stochastic Linear Dynamics by means of Multidomain Line Sampling

Mauricio A. Misraji, Marcos A. Valdebenito, Danko J. Jerez, Héctor A. Jensen, Michael Beer, Matthias G.R. Faes

PII: S0951-8320(26)00205-X
DOI: https://doi.org/10.1016/j.ress.2026.112389
Reference: RESS 112389

To appear in: *Reliability Engineering and System Safety*

Received date: 30 August 2025
Revised date: 3 February 2026
Accepted date: 7 February 2026

Please cite this article as: Mauricio A. Misraji, Marcos A. Valdebenito, Danko J. Jerez, Héctor A. Jensen, Michael Beer, Matthias G.R. Faes, First Excursion Probability Sensitivity in Stochastic Linear Dynamics by means of Multidomain Line Sampling, *Reliability Engineering and System Safety* (2025), doi: https://doi.org/10.1016/j.ress.2026.112389

First Excursion Probability Sensitivity in Stochastic Linear Dynamics by means of Multidomain Line Sampling

Mauricio A. Misraji[a,*], Marcos A. Valdebenito[a], Danko J. Jerez[b], Héctor A. Jensen[b], Michael Beer[c,e,f], Matthias G.R. Faes[a,d]

[a] *Chair for Reliability Engineering, TU Dortmund University, Leonhard-Euler-Straße 5, 44227 Dortmund, Germany*
[b] *Universidad Técnica Federico Santa María, Dept. de Obras Civiles, Av. España 1680, Valparaiso, Chile*
[c] *Institute for Risk and Reliability, Leibniz University Hannover, Callinstraße 34, 30167 Hannover, Germany*
[d] *International Joint Research Center for Engineering Reliability and Stochastic Mechanics, Tongji University, Shanghai 200092, China*
[e] *Department of Civil and Environmental Engineering, University of Liverpool, Liverpool L69 3GH, United Kingdom*
[f] *International Joint Research Center for Resilient Infrastructure & International Joint Research Center for Engineering Reliability and Stochastic Mechanics, Tongji University, Shanghai 200092, PR China*

Abstract

This contribution presents a novel framework for estimating the sensitivity of first excursion probabilities. The focus is on linear dynamic systems with non-proportional damping subject to stationary or non-stationary Gaussian excitation. The sensitivity is estimated with respect to structural parameters of the system, including material properties and geometric dimensions of the elements. In dynamical systems, calculating both the first excursion probability and its sensitivity is done in a high-dimensional space, making the task challenging and computationally expensive. In this regard, the multidomain Line Sampling framework exploits linearity to obtain sensitivity estimates as a byproduct of the first excursion probability evaluation. The results show that the presented technique is highly efficient compared to different methods in the literature, as demonstrated through two numerical examples involving small- and large-scale models.

Keywords: First excursion probability, Sensitivity analysis, Gaussian loading, Linear systems, Multidomain Line Sampling

Highlights:

- Sensitivity of failure probability estimated using multidomain Line Sampling
- Sensitivity is a byproduct of the first excursion probability
- Sensitivities of eigenvalues and eigenvectors required
- Non-proportional damping considered in the formulation

*E-mail: mauricio.misraji@tu-dortmund.de

1. Introduction

The development of stochastic models has become paramount to achieving a better understanding of the behavior of mechanical and structural systems. Stochastic representation of external loads provides a more realistic depiction of real-life phenomena. For example, stochastic processes offer more accurate representations of events like earthquakes and wind loads in structural systems, as well as vibrations and impact loads in mechanical systems. It is also noted that, in many practical cases and applications, the system reliability is dominated by the uncertainty in the excitation as commonly assumed in structural vibration serviceability, wind engineering and earthquake engineering applications (see e.g. [1] and [2]). In the context of dynamical systems, the theory of random vibrations introduces the concept of the so-called first excursion probability, which measures the chance that one or more responses of interest exceed a prescribed threshold during stochastic excitation [1]. This metric is particularly useful as a measure of serviceability [3, 4, 5] when the system behavior remains linear during stochastic excitation, allowing the response of interest to be calculated while materials operate within their linear range. To accurately estimate the first excursion probability while taking advantage of system linearity, several advanced simulation techniques have been developed considering the loading as a Gaussian process and deterministic structural models, including Efficient Importance Sampling (EIS) [6], the Domain Decomposition Method (DDM) [7], Directional Importance Sampling (DIS) [8], and multidomain Line Sampling (mLS) [9].

Although the information provided by the first excursion probability is essential for assessing system reliability [10, 11, 12, 13, 14], it is also important to study its sensitivity to possible changes in system parameters. This problem has been widely discussed in the literature [15, 16, 17, 18, 19], and two main research branches can be identified for the sensitivity of the first excursion probability [20]. The first group studies sensitivity with respect to distribution parameters of random variables [21, 22]. These parameters can include, for instance, the mean value or standard deviation of a given random variable representing uncertainty in, e.g. loading. The second group, which is the focus of this work, studies sensitivity with respect to deterministic system parameters. Methods that consider second-order moment approximations [23], combinations of stochastic simulation with Bayes' theorem for sensitivity estimates [24, 25], and the combination of stochastic simulation with local approximations of the responses of interest [26, 27, 28], are various known approaches within this group. In practical applications, system parameters such as the geomet-

ric dimensions of structural members or their elastic properties are subject to uncertainty (e.g., manufacturing tolerances), but they are still specified and controlled by the designer through nominal values. For the systems considered here, the uncertainty due to the stochastic loading is dominant, so modelling the structural parameters by their nominal values is a reasonable assumption. Accordingly, this work explicitly considers local (derivative-based) sensitivities, which provide valuable information on the magnitude of change at the nominal design, whereas global sensitivities attribute output variance to uncertain inputs and require probabilistic models for the parameters, a complementary perspective not pursued here. In this context, sensitivity is calculated as the partial derivative of the first excursion probability with respect to a system parameter. This gradient calculation involves solving an integral in a high-dimensional space, which usually has no closed-form solution.

Despite the fact that linear structural models under Gaussian loading constitute a classical setting in stochastic dynamics, the estimation of the first excursion probability sensitivities in a high-dimensional and non-stationary context remains computationally challenging and cannot be addressed with available analytical approaches. In most cases, sensitivity analysis is carried out as a post processing step that reuses the samples originally generated for reliability estimation [16, 20, 22]. Although methods such as DIS [9] and DDM [29] can compute reliability and sensitivities from the same set of model evaluations for this class of systems, their sensitivity estimators often exhibit high variance and the associated computational cost remains substantial. DIS and DDM are directional sampling methods [30, 31] that explore the standard Gaussian space along directions anchored at the origin. Line Sampling methods take a different approach, evaluating lines that need not pass through the origin, which provides an alternative way of exploring the space. One such method is mLS, whose efficiency for first excursion probability estimation has been demonstrated, and extending this approach to sensitivity estimation constitutes a natural and promising next step. Accordingly, improving sensitivity estimation is crucial, given that derivative information has broad applications in model calibration, risk evaluation, and risk-informed decision-making [10, 32, 33, 34] and, together with the first excursion probability, in reliability-based design optimization [34, 35, 2] and network applications [36].

In this work, an extension of the mLS framework for calculating the sensitivity of the first excursion probability is proposed. The methodology allows for the calculation of sensitivity estimates using mLS for both reliability and sensitivity analyses, and it is applicable to small- and

large-scale problems. The scope of the method includes linear systems subject to Gaussian loading, and the systems considered involve non-proportional damping. The latter consideration offers a more generalized methodology than the one proposed in [28], and is numerically more efficient than the methods proposed in [37, 29]. The consideration of non-proportional damping allows a closer representation of the modeled system response to real-world behavior [38]. Additionally, the special structure of the failure domain is exploited by mLS, which efficiently explores the failure domain to produce accurate and computationally inexpensive reliability and sensitivity estimates. The novelty of the proposed sensitivity extension of mLS is linked to the way exploration lines are placed relative to the elementary failure domains. Since the lines are not forced to pass through the origin and are guided by the elementary domains, they often intersect the corresponding limit-state boundary in a near-perpendicular way, which is more informative for sensitivity estimates. Directional methods such as DIS and DDM, in contrast, use rays originating at the origin, which can intersect the boundary at less informative angles and therefore require more simulations to achieve the same accuracy in sensitivity estimates. As a result, the proposed approach achieves a notable computational efficiency. Moreover, the sensitivity analysis of the spectral properties of the system is required [39], and sensitivity estimates are achieved as a byproduct of the first excursion probability estimator.

The rest of this work is organized as follows. The problem definition, together with the first excursion probability and its gradient, is presented in Section 2. Sections 3 and 4 cover the calculation of the first excursion probability and its gradient using mLS, respectively. Numerical implementation aspects are detailed in Section 5. The effectiveness of the method, including quantitative comparisons that highlight its technical advantages with respect to DIS and DDM, is demonstrated through two examples in Section 6, and finally, conclusions and future developments are discussed in Section 7.

2. Problem Statement

2.1. Gaussian Loading

The dynamic load, $\boldsymbol{p}$, applied to the system is modeled as a discrete Gaussian process of duration T, sampled at n_T time steps, each of duration Δt. The k-th time instant is defined as $t_k = (k-1)\Delta t$ for $k = 1, \ldots, n_T$. The expected value of this process at time t_k is denoted by μ_k, the k-th element of the expected value vector $\boldsymbol{\mu}$, which has dimensions $n_T \times 1$. The associated

covariance matrix, $\boldsymbol{\Sigma}$, is symmetric, bounded, and positive definite, with the covariance between t_{k_1} and t_{k_2} given by Σ_{k_1,k_2}, the (k_1, k_2)-th element of $\boldsymbol{\Sigma}$. Using the Karhunen-Loève expansion [40, 41], the elements contained in the vector of the dynamic load $\boldsymbol{p}$ are represented as:

$$p\left(t_k, \boldsymbol{z}\right) = \mu_k + \boldsymbol{\psi}_k^{\mathrm{T}} \boldsymbol{z}, \quad k = 1, \ldots, n_T, \tag{1}$$

where $p\left(t_k, \boldsymbol{z}\right)$ is the loading at time t_k, and $\boldsymbol{z}$ is a realization of a standard Gaussian random vector $\boldsymbol{Z}$ with dimensions $n_{KL} \times 1$, where n_{KL} is the truncation order of the expansion ($n_{KL} \leqslant n_T$). Solving the eigenproblem $\boldsymbol{\Sigma\Xi} = \boldsymbol{\Xi\Lambda}$ for the largest n_{KL} eigenvalues of $\boldsymbol{\Sigma}$, the matrix $\boldsymbol{\Psi} = [\boldsymbol{\psi}_1, \boldsymbol{\psi}_2, \ldots, \boldsymbol{\psi}_{n_T}]$ is obtained as $\boldsymbol{\Psi} = \boldsymbol{\Lambda}^{1/2}\boldsymbol{\Xi}^T$, where each $\boldsymbol{\psi}_k$ (of dimensions $n_{KL} \times 1$) is the K-L (Karhunen-Loève) vector associated with the time instant t_k. Without loss of generality, this work assumes $\boldsymbol{\mu} = \mathbf{0}$.

In view of this discrete formulation and time-varying excitation, classical stationary-process tools (e.g., Rice's upcrossing formulas and diffusion-based Fokker-Planck equations) are not applicable in the present setting.

2.2. Structural System

The structural system under study is linear, elastic, and damped, and it is subject to Gaussian loading $p(t, \boldsymbol{z})$. Considering n_D degrees of freedom, the system dynamics are governed by the following equation of motion [42]:

$$\boldsymbol{M}(\boldsymbol{y})\ddot{\boldsymbol{x}}(t, \boldsymbol{y}, \boldsymbol{z}) + \boldsymbol{C}(\boldsymbol{y})\dot{\boldsymbol{x}}(t, \boldsymbol{y}, \boldsymbol{z}) + \boldsymbol{K}(\boldsymbol{y})\boldsymbol{x}(t, \boldsymbol{y}, \boldsymbol{z}) = \boldsymbol{g}(\boldsymbol{y})p(t, \boldsymbol{z}), \quad t \in [0, T], \tag{2}$$

where $\boldsymbol{x}$, $\dot{\boldsymbol{x}}$, and $\ddot{\boldsymbol{x}}$ are the displacement, velocity, and acceleration vectors (dimensions $n_D \times 1$), and $\boldsymbol{M}$, $\boldsymbol{C}$, and $\boldsymbol{K}$ are the mass, damping, and stiffness matrices of dimensions $n_D \times n_D$. The load coupling vector, $\boldsymbol{g}$, also has dimensions $n_D \times 1$, while the vector $\boldsymbol{y}$, with dimensions $n_Y \times 1$, contains the so-called structural design parameters. This vector groups parameters of the system under study which can be modified, such as geometric dimensions of beams. In the present work, $\boldsymbol{y}$ is treated as a deterministic vector of nominal design values controlled by the designer, while the uncertainty is represented solely by the stochastic excitation. The alternative formulation, in which uncertainties in these structural parameters are modelled explicitly by random variables and their distribution parameters, corresponds to the first branch of sensitivity methods discussed in Section 1 and is not further pursued here. Therefore, to account for systems with non-proportional

damping, Equation (2) can be reformulated in an augmented form [43]:

$$\underbrace{\left[\begin{array}{c:c} \mathbf{0}_{n_D\times n_D} & \boldsymbol{M}(\boldsymbol{y}) \\ \hdashline \boldsymbol{M}(\boldsymbol{y}) & \boldsymbol{C}(\boldsymbol{y}) \end{array}\right]}_{[\boldsymbol{M}_a(\boldsymbol{y})]} \underbrace{\left\{\begin{array}{c} \ddot{\boldsymbol{x}}(t,\boldsymbol{y},\boldsymbol{z}) \\ \hdashline \dot{\boldsymbol{x}}(t,\boldsymbol{y},\boldsymbol{z}) \end{array}\right\}}_{\{\dot{\boldsymbol{q}}(t,\boldsymbol{y},\boldsymbol{z})\}} + \underbrace{\left[\begin{array}{c:c} -\boldsymbol{M}(\boldsymbol{y}) & \mathbf{0}_{n_D\times n_D} \\ \hdashline \mathbf{0}_{n_D\times n_D} & \boldsymbol{K}(\boldsymbol{y}) \end{array}\right]}_{[\boldsymbol{K}_a(\boldsymbol{y})]} \underbrace{\left\{\begin{array}{c} \dot{\boldsymbol{x}}(t,\boldsymbol{y},\boldsymbol{z}) \\ \hdashline \boldsymbol{x}(t,\boldsymbol{y},\boldsymbol{z}) \end{array}\right\}}_{\{\boldsymbol{q}(t,\boldsymbol{y},\boldsymbol{z})\}} = \underbrace{\left\{\begin{array}{c} \mathbf{0}_{n_D\times 1} \\ \hdashline \boldsymbol{g}(\boldsymbol{y}) \end{array}\right\}}_{\{\boldsymbol{g}_a(\boldsymbol{y})\}} p(t,\boldsymbol{z}), \tag{3}$$

or more compactly as:

$$[\boldsymbol{M}_a(\boldsymbol{y})]\,\{\dot{\boldsymbol{q}}(t,\boldsymbol{y},\boldsymbol{z})\} + [\boldsymbol{K}_a(\boldsymbol{y})]\,\{\boldsymbol{q}(t,\boldsymbol{y},\boldsymbol{z})\} = \{\boldsymbol{g}_a(\boldsymbol{y})\}\,p(t,\boldsymbol{z}), \tag{4}$$

where $\{\boldsymbol{q}\}$ is a vector that contains both system velocities and displacements, with dimensions $2n_D \times 1$; $[\boldsymbol{M}_a]$ and $[\boldsymbol{K}_a]$ are the augmented mass and stiffness matrices, each with dimensions $2n_D \times 2n_D$; and $\{\boldsymbol{g}_a\}$ is the augmented load coupling vector, with dimensions $2n_D \times 1$. Note that, within the scope of this work, the number of degrees of freedom n_D is large (e.g., in the order of tens of thousands). As a consequence, diffusion-theory approaches based on the Fokker-Planck-Kolmogorov (FPK) equation are not feasible for the state-space formulation in Equation (4), since they would require solving a prohibitively high-dimensional PDE in the $2n_D$-dimensional state space.

Key dynamic responses, such as displacements, accelerations, internal stresses, or their linear combinations, are represented by $\eta_i(t,\boldsymbol{y},\boldsymbol{z})$ for $i = 1,\ldots,n_\eta$, and can be computed using the convolution integral [42]:

$$\eta_i(t,\boldsymbol{y},\boldsymbol{z}) = \int_0^t h_i(t-\tau,\boldsymbol{y})\,p(\tau,\boldsymbol{z})\,d\tau, \quad i = 1,\ldots,n_\eta, \tag{5}$$

where $h_i(t,\boldsymbol{y})$ is the unit impulse response function of the i-th response. Here, $p(t,\boldsymbol{z})$ refers to the Gaussian load, and zero initial conditions are assumed, i.e., $\boldsymbol{x}(0,\boldsymbol{y},\boldsymbol{z}) = \dot{\boldsymbol{x}}(0,\boldsymbol{y},\boldsymbol{z}) = \mathbf{0}_{n_D\times 1}$. Note that solving Equation (4) through modal decomposition enables expressing the response of interest as a combination of the vector $\boldsymbol{q}(t,\boldsymbol{y},\boldsymbol{z})$, such that $\eta_i(t,\boldsymbol{y},\boldsymbol{z}) = \boldsymbol{\gamma}_i^T\boldsymbol{q}(t,\boldsymbol{y},\boldsymbol{z})$, where $\boldsymbol{\gamma}_i$ is a constant vector with dimensions $2n_D \times 1$. Furthermore, as depicted in e.g., [44], the unit impulse response function of the i-th response of interest is expressed as:

$$h_i(t,\boldsymbol{y}) = \sum_{r=1}^{2n_D} \frac{\boldsymbol{\gamma}_i^T\boldsymbol{\phi}_r(\boldsymbol{y})\boldsymbol{\phi}_r(\boldsymbol{y})^T\boldsymbol{g}_a(\boldsymbol{y})}{\boldsymbol{\phi}_r(\boldsymbol{y})^T\boldsymbol{M}_a(\boldsymbol{y})\boldsymbol{\phi}_r(\boldsymbol{y})} e^{\lambda_r(\boldsymbol{y})t}, \quad i = 1,\ldots,n_\eta, \tag{6}$$

where $\boldsymbol{\phi}_r(\boldsymbol{y})$ and $\lambda_r(\boldsymbol{y})$ represent the eigenvectors and eigenvalues, respectively, associated with Equation (4). Note that Equation (6) is only valid if $\boldsymbol{C}$ is symmetric; otherwise, the right and left eigenvector problems need to be considered. In cases where n_D is large, model truncation [42] can be applied to Equation (6) to simplify the calculation or reduce computational effort by selecting a subset of eigenvectors and eigenvalues smaller than $2n_D$.

The Gaussian loading defined in Section 2.1 is discretized with respect to time. Consequently, the i-th response of interest at the time instant t_k can be approximated by discretizing the integral in Equation (5), as follows:

$$\eta_i\left(t_k, \boldsymbol{y}, \boldsymbol{z}\right) = \boldsymbol{a}_{i,k}(\boldsymbol{y})^T \boldsymbol{z}, i = 1, \ldots, n_\eta, k = 1, \ldots, n_T, \tag{7}$$

where the vector $\boldsymbol{a}_{i,k}(\boldsymbol{y})$ of dimensions $n_{KL} \times 1$ is defined as:

$$\boldsymbol{a}_{i,k}(\boldsymbol{y}) = \sum_{m=1}^{k} \Delta t \epsilon_m h_i\left(t_k - t_m, \boldsymbol{y}\right) \boldsymbol{\psi}_m, \tag{8}$$

where the parameter ϵ_m is determined by the chosen integration scheme. For instance, in the case of the trapezoidal scheme, $\epsilon_m = 1/2$ when $m = 1$ or $m = k$, and $\epsilon_m = 1$ otherwise [45]. It is important to highlight that, in Equation (7), the vector $\boldsymbol{z}$ is associated with the Gaussian load $\boldsymbol{p}$, while the dependency on the design vector $\boldsymbol{y}$ is exclusively linked to the structural model through the vector $\boldsymbol{a}_{i,k}$.

2.3. First Excursion Probability

The reliability of the system can be assessed by quantifying its performance. This is achieved by comparing the responses of interest, $\eta_i(t)$, $i = 1, \ldots, n_\eta$, with the corresponding design requirements, b_i, $i = 1, \ldots, n_\eta$, over time. This comparison is represented mathematically by the performance function $g(\boldsymbol{y}, \boldsymbol{z})$, which determines whether the response of interest exceeds a prescribed threshold during the action of the loading over time. The performance function is defined as follows:

$$g(\boldsymbol{y}, \boldsymbol{z}) = 1 - \max_{i=1,\ldots,n_\eta} \left(\max_{k=1,\ldots,n_T} \left(\frac{\left|\eta_i\left(t_k, \boldsymbol{y}, \boldsymbol{z}\right)\right|}{b_i} \right) \right), \tag{9}$$

where $|\cdot|$ is the absolute value. The system is considered to fail when the performance function is negative, while a positive value indicates that the design requirements are met. Note that all possible realizations of the Gaussian vector $\boldsymbol{z}$ that lead to failure, for a given design vector $\boldsymbol{y}$, define

the failure domain. This domain can be formally expressed as: $F = \{\boldsymbol{z} \in \mathbb{R}^{n_{KL}} : g(\boldsymbol{y}, \boldsymbol{z}) \leqslant 0\}$.

The so-called first excursion probability [1] quantifies the probability associated with the failure domain and is given by:

$$p_F(\boldsymbol{y}) = \int_{g(\boldsymbol{y},\boldsymbol{z})\leq 0} f_{\boldsymbol{Z}}(\boldsymbol{z}) d\boldsymbol{z}, \tag{10}$$

where $f_{\boldsymbol{Z}}(\boldsymbol{z})$ represents the standard Gaussian probability density function in n_{KL}-dimensional space.

The first excursion probability integral can be challenging to solve. Specifically, as n_{KL} increases, the integral becomes high-dimensional and does not have a closed-form solution. In this case, the integral must be estimated using advanced simulation techniques [46]. To address this, within the context of this work, advanced simulation methods have been developed that take advantage of the system linearity to estimate the first excursion probability [6, 7, 8, 9].

2.4. Geometry of the Failure Domain

The failure domain defined in Section 2.3 has a very special structure. Analyzing Equation (9), it is evident that it can be decomposed into $n_\eta n_T$ *elementary failure domains*. This characteristic arises from the linearity of the system and the chosen representation method for the Gaussian loading [6, 47]. The elementary failure domains, denoted as $F_{i,k}$, represent the event where the response of interest η_i exceeds the design value b_i at the specific time instant t_k. The subset that includes positive values of the response of interest exceeding b_i is defined as $F_{i,k}^{+} = \left\{\boldsymbol{z} \in \mathbb{R}^{n_{KL}} : \boldsymbol{a}_{i,k}^T(\boldsymbol{y})\boldsymbol{z} \geqslant b_i\right\}$. Similarly, the subset representing negative values of the response of interest falling below $-b_i$ is defined as $F_{i,k}^{-} = \left\{\boldsymbol{z} \in \mathbb{R}^{n_{KL}} : \boldsymbol{a}_{i,k}^T(\boldsymbol{y})\boldsymbol{z} \leqslant -b_i\right\}$. The above definitions allow the failure domain to be expressed as the union of the elementary failure domains:

$$F = \bigcup_{i=1}^{n_\eta} \bigcup_{k=1}^{n_T} F_{i,k}, \tag{11}$$

where $F_{i,k} = F_{i,k}^{+} \cup F_{i,k}^{-}$. Furthermore, the limit state function related to the elementary failure domain $F_{i,k}$ is denoted as $g_{i,k}$. In the same manner, the limit state function associated with $F_{i,k}^{+}$ is denoted by $g_{i,k}^{+}$, whereas the limit state function associated with $F_{i,k}^{-}$ is denoted by $g_{i,k}^{-}$. Figure 1 illustrates a representation of the elementary failure domains for the case where $n_\eta = 1$ and $n_T = n_{KL} = 2$. Note that the domains are constrained to the box boundaries, which is just for drawing purposes, as in reality z_1 and z_2 cover all the real line. The domains $F_{1,1}$ and $F_{1,2}$ are divided into their positive and negative parts, as schematically shown in Figure 1(b). Zones where

overlap occurs between the elementary failure domains can be identified, which indicates that the response of interest exceeds the threshold at both time instants simultaneously. Furthermore, although this is a bidimensional representation of the problem, the overlap between elementary failure domains can be significant, which provides insights into the high level of interaction that exists in a higher-dimensional case.

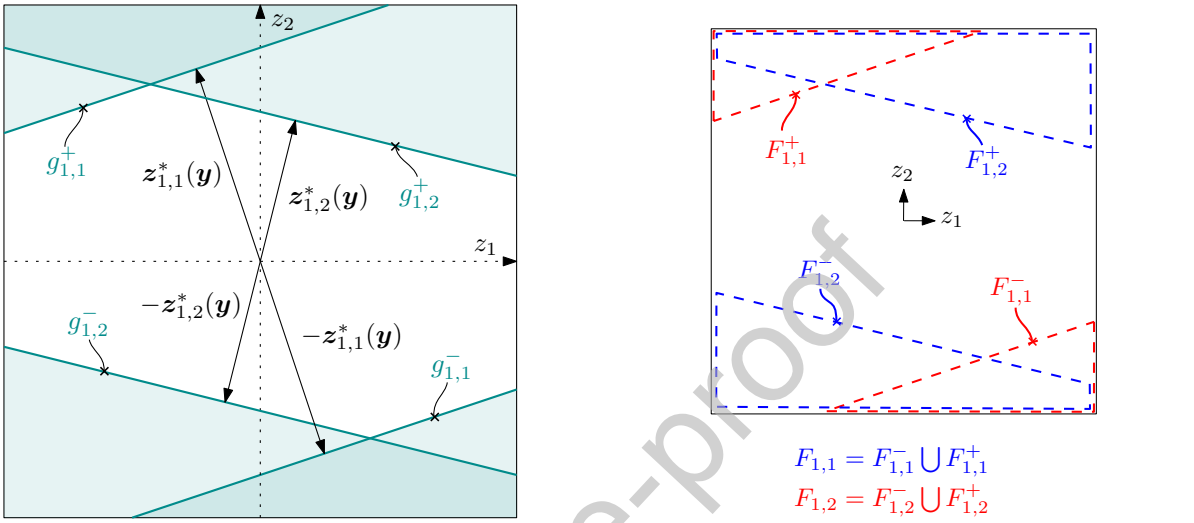

(a) Performance functions and design points associated with F_1 and F_2.

(b) Geometrical description of the elementary failure domains F_1 and F_2 shown in (a).

Figure 1: Elementary failure domains representation for the case where $n_\eta = 1$ and $n_T = n_{KL} = 2$.

The spatial definition of each elementary failure domain is given by the so-called design point [6, 47, 48]. This corresponds to the realization of $\boldsymbol{z}$ within the elementary failure domain with the highest likelihood, or equivalently, to the point with the smallest Euclidean norm from the origin to a realization of $\boldsymbol{z}$ within the elementary failure domain, which is given by [6, 47]:

$$\boldsymbol{z}^*_{i,k}(\boldsymbol{y}) = b_i \frac{\boldsymbol{a}_{ik}(\boldsymbol{y})}{\|\boldsymbol{a}_{i,k}(\boldsymbol{y})\|^2}, \quad i = 1, \ldots, n_\eta, \quad k = 1, \ldots, n_T, \tag{12}$$

where $\boldsymbol{z}^*_{i,k}(\boldsymbol{y})$ is the design point associated with the $F^+_{i,k}$ elementary failure domain, as illustrated in Figure 1a. The Euclidean norm of this vector is known as the reliability index, which is given by [6, 47]:

$$\beta_{i,k}(\boldsymbol{y}) = \frac{b_i}{\|\boldsymbol{a}_{i,k}(\boldsymbol{y})\|}, \quad i = 1, \ldots, n_\eta, \quad k = 1, \ldots, n_T, \tag{13}$$

being the reliability index $\beta_{i,k}(\boldsymbol{y})$ associated with the positive $F^+_{i,k}$ and negative $F^-_{i,k}$ elementary failure domains. Therefore, due to the linearity of the performance functions in the Gaussian space, calculating the probability of occurrence for each elementary domain is straightfor-

ward: $P[F_{i,k}^{+}] = P[F_{i,k}^{-}] = \Phi[-\beta_{i,k}]$, where $P[\cdot]$ denotes probability and $\Phi[\cdot]$ represents the one-dimensional Gaussian cumulative distribution function [6, 47]. An upper bound $\hat{p}_F$ of the failure probability [6] is given by:

$$\widehat{p}_F = \sum_{i=1}^{n_\eta} \sum_{k=1}^{n_T} P\left[F_{i,k}\right] = 2 \sum_{i=1}^{n_\eta} \sum_{k=1}^{n_T} \Phi\left(-\beta_{i,k}\right). \tag{14}$$

Please note that the upper bound $\hat{p}_F$ would become equal to the failure probability only in the hypothetical case where there is no overlap between elementary failure domains. But this case is not observed in practical cases and hence, $\hat{p}_F$ is an upper bound for p_F.

2.5. Gradient of the First Excursion Probability

The sensitivity of the first excursion probability can be assessed from Equation (10) due to its dependence on the design vector $\boldsymbol{y}$. One possible way to evaluate this sensitivity is by determining the gradient of the first excursion probability (as described in Appendix A):

$$\frac{\partial p_F(\boldsymbol{y})}{\partial y_q} = -\int_{g(\boldsymbol{y},\boldsymbol{z})=0} \frac{\partial g(\boldsymbol{y},\boldsymbol{z})}{\partial y_q} \frac{1}{\|\nabla_{\boldsymbol{z}} g(\boldsymbol{y},\boldsymbol{z})\|} f_{\boldsymbol{Z}}(\boldsymbol{z}) dS, \quad q = 1, \ldots, n_Y, \tag{15}$$

where $\|\cdot\|$ denotes the Euclidean norm, $\nabla_{\boldsymbol{z}}$ is the nabla operator $\nabla_{\boldsymbol{z}} = [\partial/\partial z_1, \ldots, \partial/\partial z_{n_{KL}}]^T$, and dS is a differential element of the limit state hypersurface $S = \{\boldsymbol{z} \in \mathbb{R}^{n_{KL}} : g(\boldsymbol{y},\boldsymbol{z}) = 0\}$. However, evaluating the expression in Equation (15) is challenging, as it requires solving a $(n_{KL}-1)$-dimensional integral. To address this issue, an advanced simulation technique based on multidomain Line Sampling is introduced in Section 3 for estimating the integral.

3. First Excursion Probability Estimation

3.1. General Remarks

The first excursion probability is evaluated by reformulating the integral in Equation (10) in terms of the *effective contribution* of each elementary failure domain to the overall failure probability. This formulation builds upon Line Sampling [49] and its multidomain extension [9]. In the following, the fundamentals of multidomain Line Sampling are explained in detail. Please note that the description presented here differs slightly from that in [9] to facilitate implementation.

3.2. Effective Contribution of the Elementary Failure Domains

The first excursion probability integral shown in Equation (10) can be very challenging. This is due to the difficulty in analytically characterizing the shape of the failure domain. As shown in Section 2.4, the analytical definition of each elementary failure domain provides valuable information for assessing the first excursion probability. Therefore, the failure probability integral in Equation (10) can be expressed in terms of the contributions of each elementary failure domain [6, 9], as follows:

$$p_F(\boldsymbol{y}) = \sum_{i=1}^{n_\eta} \sum_{k=1}^{n_T} p_{i,k}(\boldsymbol{y}), \tag{16}$$

where $p_{i,k}$, known as the *effective contribution*, is related to the elementary failure domain $F_{i,k}$ and is defined as follows:

$$p_{i,k}(\boldsymbol{y}) = \int_{\boldsymbol{z} \in F_{i,k}} \frac{1}{\sum_{h=1}^{n_\eta} \sum_{j=1}^{n_T} I_{F_{h,j}}(\boldsymbol{y}, \boldsymbol{z})} f_Z(\boldsymbol{z}) d\boldsymbol{z}. \tag{17}$$

The term $I_{F_{h,j}}(\boldsymbol{y}, \boldsymbol{z})$ is an indicator function which is equal to 1 in case that $\boldsymbol{z} \in F_{h,j}$ and 0 otherwise.

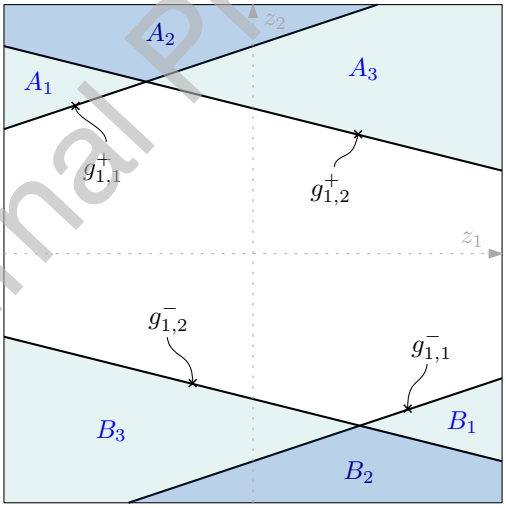

Figure 2: Elementary failure domains representation for the case where $n_\eta = 1$ and $n_T = n_{KL} = 2$.

The effective contribution of each elementary failure domain can be calculated by decomposing the failure domains into zones that exhibit varying levels of interaction between the elementary failure domains. This is illustrated schematically in Figure 2 for the particular case where $n_\eta = 1$ and $n_T = n_{KL} = 2$. As shown in Figure 2, the subsets of the failure domain denoted by A_1, A_3, B_1, and B_3 are defined by a single elementary failure domain each, without exhibiting any

overlap. The remaining subsets, A_2 and B_2, are defined by two elementary failure domains each, exhibiting overlap between them. To understand the definition of effective contribution, consider the calculation of $p_{1,2}$ in the example shown in Figure 2. The integral from Equation (17) can be separated over the domains A_2, A_3, B_2 and B_3. The *discounting factor* $1/\sum_{h=1}^{n_\eta}\sum_{j=1}^{n_T} I_{F_{h,j}}(\boldsymbol{y},\boldsymbol{z})$, from Equation (17), accounts for discounting the effective contribution resulting from the interaction between elementary failure domains. Then, the discounting factor value is equal to 1 when integrating over domains A_3 and B_3, and equal to 1/2 when integrating over domains A_2 and B_2. Therefore, it is straightforward to note that, in Equation (17), the contribution to the failure probability from the region where elementary failure domains overlap is accounted for half in the calculation of $p_{1,1}$ and half in $p_{1,2}$. Consequently, the effective contribution $p_{i,k}$ is given by the probability of occurrence of the event $F_{i,k}$, adjusted by a discounting factor that accounts for the overlap between elementary failure domains. Thus, the addition of all effective contributions $p_{i,k}$ over all responses η_i, $i = 1, \ldots, n_\eta$ and over all time instants t_k, $k = 1, \ldots, n_T$, provides the sought failure probability $p_F(\boldsymbol{y})$ as shown in Equation (16).

3.3. Multidomain Line Sampling Formulation

The first excursion probability is calculated based on the effective contributions of the elementary failure domains, which are estimated using Line Sampling, a simulation approach well documented in the literature, see e.g. [49]. Therefore, in the following, it is assumed that the reader is familiar with basic concepts of Line Sampling such as the important direction $\boldsymbol{\alpha}$, rotation of the associated coordinate system, etc. Nevertheless and for the sake of completeness, some basic concepts of Line Sampling are described in Appendix B. The extension of Line Sampling to cases where the failure domain has the special structure presented in Section 2.4 is known as multidomain Line Sampling [9]. To understand its formulation, each elementary failure domain is now associated with an important direction, defined as:

$$\boldsymbol{\alpha}_{i,k} = \frac{\boldsymbol{z}^*_{i,k}(\boldsymbol{y})}{||\boldsymbol{z}^*_{i,k}(\boldsymbol{y})||}, \tag{18}$$

where $\boldsymbol{\alpha}_{i,k}$ is a vector of unit Euclidean norm, pointing in the direction of the design point of the (i,k)-th elementary failure domain. Note that whether the vector points towards $F^+_{i,k}$ or $F^-_{i,k}$ does not affect the formulation of the method. Now, it is possible to define a rotated coordinate system

associated with the elementary failure domain $F_{i,k}$ as:

$$\boldsymbol{z} = \boldsymbol{R}_{i,k}\boldsymbol{z}_{i,k}^{\perp} + \boldsymbol{\alpha}_{i,k} z_{i,k}^{\parallel}, \tag{19}$$

where $\boldsymbol{R}_{i,k}$ is an $n \times (n-1)$ matrix; $\boldsymbol{z}_{i,k}^{\perp}$ is an $(n-1)$-dimensional vector representing the coordinates in the hyperplane orthogonal to $\boldsymbol{\alpha}_{i,k}$; and $z^{\parallel}$ is a scalar representing the coordinate along the direction parallel to $\boldsymbol{\alpha}_{i,k}$. The orthonormal basis of the new coordinate system is defined by the square matrix $[\boldsymbol{R}_{i,k}, \boldsymbol{\alpha}_{i,k}]$. Then, $z_{i,k}^{\parallel}$ follows a one-dimensional standard Gaussian distribution, while $\boldsymbol{z}_{i,k}^{\perp}$ is associated with a standard Gaussian distribution in $(n-1)$ dimensions. Note that the dependence on $\boldsymbol{y}$ is omitted for $\boldsymbol{\alpha}_{i,k}$ and $\boldsymbol{R}_{i,k}$, as the coordinate system and the associated definitions are kept fixed for the subsequent calculations in this contribution (evaluated at the current design). Figure 3 illustrates the important directions $\boldsymbol{\alpha}_{1,1}$ and $\boldsymbol{\alpha}_{1,2}$, as well as a rotated system generated according to $F_{1,2}$, for the case where $n_\eta = 1$ and $n_{KL} = n_T = 2$. The axes $z_{1,2}^{\parallel}$ and $z_{1,2}^{\perp}$ indicate the parallel and perpendicular directions with respect to $F_{1,2}$. The boundaries of the failure and safe domains are also shown.

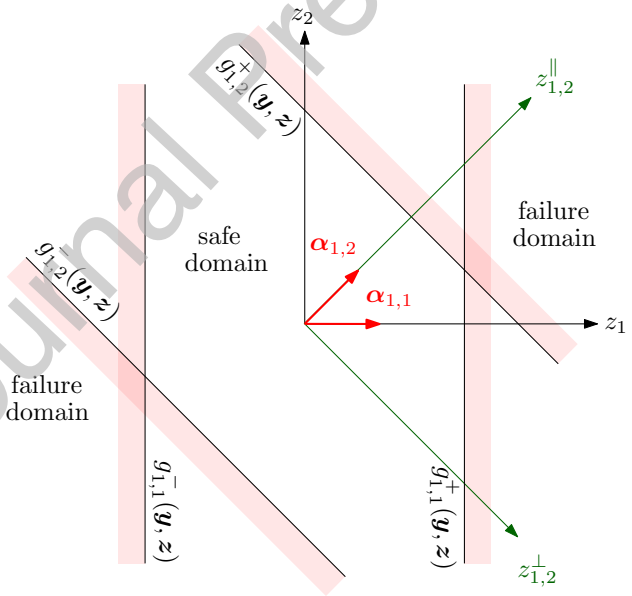

Figure 3: Schematic representation of the multidomain Line Sampling technique.

The rotated coordinate system from Equation (19) allows the effective contribution integral from Equation (17) to be expressed as follows:

$$p_{i,k}(\boldsymbol{y}) = \int_{\Omega_{i,k}^{\perp}} \int_{\Omega_{i,k}^{\parallel}(\boldsymbol{y})} \frac{1}{\sum_{h=1}^{n_\eta}\sum_{j=1}^{n_T} I_{F_{h,j}}\left(\boldsymbol{R}_{i,k}\boldsymbol{z}_{i,k}^{\perp} + \boldsymbol{\alpha}_{i,k} z_{i,k}^{\parallel}\right)} f_{Z_{i,k}^{\parallel}}\left(z_{i,k}^{\parallel}\right) f_{\boldsymbol{Z}_{i,k}^{\perp}}\left(\boldsymbol{z}_{i,k}^{\perp}\right) dz_{i,k}^{\parallel} d\boldsymbol{z}_{i,k}^{\perp}, \tag{20}$$

where $\Omega_{i,k}^{\perp} = \left\{ \boldsymbol{z}_{i,k}^{\perp} \in \mathbb{R}^{(n_{KL}-1)} \right\}$ and $\Omega_{i,k}^{\parallel}(\boldsymbol{y}) = \left\{ z_{i,k}^{\parallel} \in \mathbb{R}^1 : |\boldsymbol{a}_{i,k}^T(\boldsymbol{y})\boldsymbol{z}| \geqslant b_i \right\}$ are introduced to simplify the notation. The above integral requires integration along a line that accounts for the interaction between different elementary failure domains. Therefore, Equation (20) provides an expression for calculating the effective contribution to the failure probability using multidomain Line Sampling.

3.4. First Excursion Probability by means of Multidomain Line Sampling

The estimation of the first excursion probability using Equation (16) presents two important challenges. First, Equation (20) requires the calculation of its inner integral, which can be computed analytically, a procedure that is explained later in Section 5.3. Second, Equation (16) requires the calculation of all the effective contribution terms $p_{i,k}$, where $n_\eta n_T$ can be on the order of thousands. This can be highly computationally demanding. To address this issue, the summation in Equation (16) can be estimated through simulation [7], leading to:

$$p_F(\boldsymbol{y}) = \sum_{i=1}^{n_\eta} \sum_{k=1}^{n_T} \left(\frac{1}{\omega_{i,k}} p_{i,k}(\boldsymbol{y}) \right) \omega_{i,k}, \tag{21}$$

where $\omega_{i,k}, i = 1, \ldots, n_\eta, k = 1, \ldots, n_T$ correspond to weight factors such that $\omega_{i,k} > 0$ and $\sum_{i=1}^{n_\eta} \sum_{k=1}^{n_T} \omega_{i,k} = 1$. These weights can be chosen using different criteria. A good choice is to rank the importance of the effective contributions to the failure probability in proportion to the failure probability of their respective elementary failure domains. Therefore, the weights in Equation (21) play the role of a probability mass function, which is defined as [6]:

$$\omega_{i,k} = \frac{P\left[F_{i,k}\right]}{\sum_{h=1}^{n_\eta} \sum_{j=1}^{n_T} P\left[F_{h,j}\right]}. \tag{22}$$

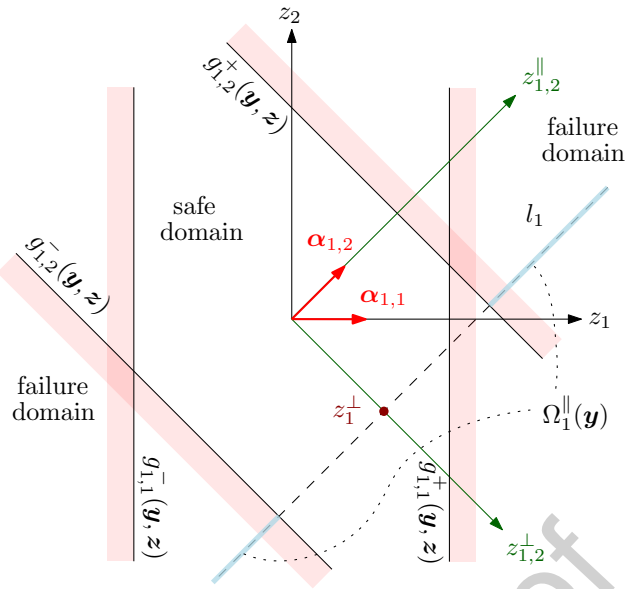

Figure 4: Schematic representation of the multidomain Line Sampling technique, including one sample realization $z_1^{\perp}$ (dark red), its associated line l_1 (black dashed line), and domain $\Omega_1^{\parallel}(\boldsymbol{y})$ (light blue).

The first excursion probability in Equation (21) now involves the summation of a discrete random variable and integration over various continuous random variables. By simulating both types of random variables, the first excursion probability can be estimated as:

$$\tilde{p}_F = \frac{1}{N}\sum_{j=1}^{N}\left(\frac{1}{\omega_{s_j}}\,\tilde{p}_{s_j}\left(\boldsymbol{y},\boldsymbol{z}_j^{\perp}\right)\right). \tag{23}$$

Here, $\tilde{p}_F$ is an estimate of p_F; N represents the total number of samples; for each $j = 1,\ldots,N$, an index s_j is independently sampled from the set $I = \{1,\ldots,n_\eta n_T\}$ according to the probability mass function ω_{s_j}. Each s_j uniquely corresponds to a pair (i,k), thereby identifying a particular elementary failure domain, i.e., variables that depend on a pair (i,k), such as $\boldsymbol{\alpha}_{i,k}$, are written as $\boldsymbol{\alpha}_{s_j}$; the vector $\boldsymbol{z}_j^{\perp}$ follows a $(n_{KL}-1)$-dimensional standard multivariate Gaussian distribution and is always defined with respect to the coordinate system associated with the selected domain s_j for sample j; and $\tilde{p}_{s_j}$ denotes the estimate of the effective contribution evaluated at $\boldsymbol{y}$ and $\boldsymbol{z}_j^{\perp}$. The quantity $\tilde{p}_{s_j}$ can be calculated as:

$$\tilde{p}_{s_j}(\boldsymbol{y},\boldsymbol{z}_j^{\perp}) = \int_{\Omega_j^{\parallel}(\boldsymbol{y})} \frac{1}{\sum_{h=1}^{n_\eta}\sum_{l=1}^{n_T} I_{F_{h,l}}\left(\boldsymbol{R}_{s_j}\boldsymbol{z}_j^{\perp} + \boldsymbol{\alpha}_{s_j} z_j^{\parallel}\right)} f_{Z^{\parallel}_{s_j}}\left(z_j^{\parallel}\right)\, dz_j^{\parallel}. \tag{24}$$

where $\Omega_j^{\parallel}(\boldsymbol{y})$ is the portion of the failure domain lying on the line $l_j = \left\{\boldsymbol{R}_{s_j}\,\boldsymbol{z}_j^{\perp} + \boldsymbol{\alpha}_{s_j}\,z_j^{\parallel} \;\middle|\; z_j^{\parallel} \in \mathbb{R}\right\}$;

that is, $\Omega_j^{\parallel}(\boldsymbol{y}) = l_j \cap F_{s_j}$. In the same manner, the positive and negative portions of the domain can be defined as $\Omega_j^{+,\parallel}(\boldsymbol{y}) = l_j \cap F_{s_j}^{+}$ and $\Omega_j^{-,\parallel}(\boldsymbol{y}) = l_j \cap F_{s_j}^{-}$, respectively. It is important to note that the integral in Equation (24) must be evaluated along a line corresponding to a possible realization of the random variable $\boldsymbol{z}_j^{\perp}$. This is depicted in Figure 4, where the sample $j = 1$ selects the domain index s_1 corresponding to the pair $(i, k) = (1, 2)$. Thus, the realization $z_1^{\perp}$ is represented as a dark red point, together with its corresponding line l_1 (black dashed line), both defined with respect to the coordinate system of $F_{1,2}$. The light blue region indicates the domain $\Omega_1^{\parallel}(\boldsymbol{y})$ associated with this sample, whose associated numerical integration is explained in detail in Section 5.3. Therefore, Equation (23) defines the first excursion probability estimator based on *multidomain Line Sampling* [9].

It is straightforward to derive that the coefficient of variation, δ_{p_F}, associated with the first excursion probability estimator in Equation (23) is given by:

$$\delta_{p_F} = \frac{1}{\tilde{p}_F(\boldsymbol{y})} \sqrt{\frac{1}{N(N-1)} \sum_{j=1}^{N} \left(\left(\frac{1}{\omega_{s_j}} \tilde{p}_{s_j}(\boldsymbol{y}, \boldsymbol{z}_j^{\perp}) \right) - \tilde{p}_F(\boldsymbol{y}) \right)^2} \tag{25}$$

4. Sensitivity Estimation of First Excursion Probability

4.1. General Remarks

This contribution extends the multidomain Line Sampling [9] technique, originally developed for the calculation of first-excursion probabilities in linear systems subject to Gaussian loading, to also provide an estimator for the sensitivity of the first excursion probability. The calculation of the first excursion probability sensitivity, as shown in Equation (15), requires the calculation of an integral over the limit state hypersurface. The literature suggests that estimating this quantity can be done, for example, by methods such as Directional Sampling [15] and Line Sampling [50]. The unique configuration of the failure domain, as described in Equation (9), motivates the development of specialized methods to address this challenge, with the present work being one such contribution.

4.2. Sensitivity of the First Excursion Probability by means of Multidomain Line Sampling

The sensitivity of the first excursion probability can be obtained by calculating the derivative of the effective contributions from Equation (16) with respect to a design parameter y_q, leading

to:

$$\frac{\partial p_F(\boldsymbol{y})}{\partial y_q} = \sum_{i=1}^{n_\eta} \sum_{k=1}^{n_T} \frac{\partial p_{i,k}(\boldsymbol{y})}{\partial y_q}, \tag{26}$$

where $\partial(\cdot)/\partial y_q$ denotes the partial derivative with respect to the design parameter y_q. The influence of changes in the effective contributions due to a perturbation Δ in the design parameter y_q is illustrated schematically in Figure 5, for the case where $n_\eta = 1$, $n_T = n_{KL} = 2$, $n_Y = 1$, and the design parameter y_q is perturbed. The limit state functions without perturbation of the design parameter are denoted by $g_{1,1}(y_q, \boldsymbol{z})$ and $g_{1,2}(y_q, \boldsymbol{z})$, while the perturbed limit state functions are represented as $g_{1,1}(y_q + \Delta, \boldsymbol{z})$ and $g_{1,2}(y_q + \Delta, \boldsymbol{z})$, in both cases associated with the elementary failure domains $F_{1,1}$ and $F_{1,2}$, respectively. A sample $j = 1$ is generated according to the pair $(i, k) = (1, 2)$ in order to estimate the effective contribution $p_{1,2}$, which is approximated by $\tilde{p}_1$ using Equation (24). In this case, it is necessary to perform an integration over a portion of the line l_1. The perturbation Δ induces changes in the limit state functions of the elementary failure domains and, as a consequence, affects both the portion of the integration over the line l_1, which is now represented by the domain $\Omega_1^{\parallel}(y_q + \Delta)$ (shown as a light blue line), and the length of the segments with different degrees of overlap. Therefore, the sensitivity of the effective contributions quantifies these changes with respect to a specific design parameter y_q and can be calculated directly from Equation (20), leading to:

$$\frac{\partial p_{i,k}(\boldsymbol{y})}{\partial y_q} = \int_{\Omega_{i,k}^{\perp}} \frac{\partial}{\partial y_q} \left(\int_{\Omega_{i,k}^{\parallel}} \frac{1}{\sum_{h=1}^{n_\eta} \sum_{j=1}^{n_T} I_{F_{h,j}} \left(\boldsymbol{R}_{i,k} \boldsymbol{z}_{i,k}^{\perp} + \boldsymbol{\alpha}_{i,k} z_{i,k}^{\parallel} \right)} f_{Z_{i,k}^{\parallel}} \left(z_{i,k}^{\parallel} \right) dz_{i,k}^{\parallel} \right) f_{\boldsymbol{Z}_{i,k}^{\perp}} \left(\boldsymbol{z}_{i,k}^{\perp} \right) d\boldsymbol{z}_{i,k}^{\perp}. \tag{27}$$

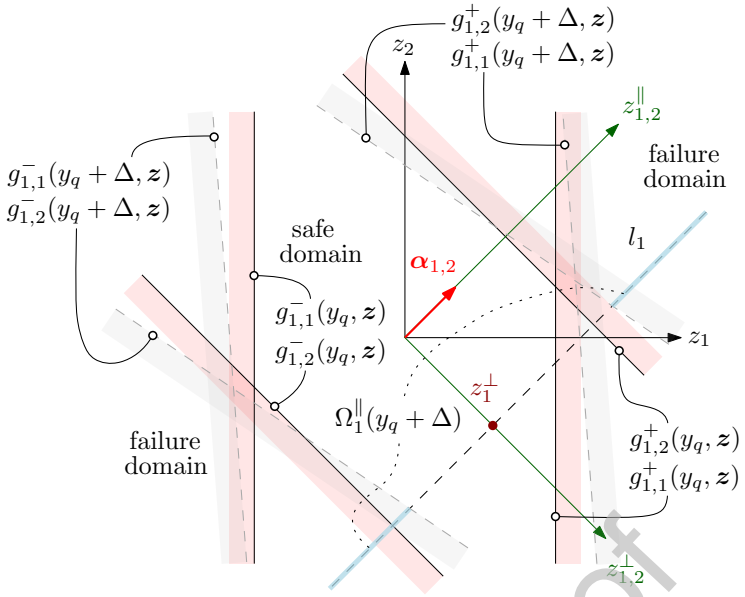

Figure 5: Schematic representation for the sensitivity of the effective contributions for the case where $n_\eta = 1$, $n_T = n_{KL} = 2$ and $n_Y = 1$.

The estimation of the sensitivity of the first excursion probability using Equation (26) presents two important challenges, in the same way as Equation (16). First, the inner integral in Equation (27) is computed analytically, a procedure that is explained later in Section 5.3. Second, Equation (16) requires the calculation of all the partial derivatives of the effective contribution terms $\partial p_{i,k}(\boldsymbol{y})/\partial y_q$, where $n_\eta n_T$ can be on the order of thousands. This may incur a high computational cost. To address this issue, the summation in Equation (26) can be estimated through simulation [7] as in Section 3.4, resulting in:

$$\frac{\partial p_F(\boldsymbol{y})}{\partial y_q} = \sum_{i=1}^{n_\eta}\sum_{k=1}^{n_T}\left(\frac{1}{\omega_{i,k}}\frac{\partial p_{i,k}(\boldsymbol{y})}{\partial y_q}\right)\omega_{i,k}, \tag{28}$$

where $\omega_{i,k}$ is defined in Equation (22). The sensitivity of the first excursion probability in Equation (28) now involves the summation of a discrete random variable and integration over various continuous random variables. By simulating both types of random variables, the sensitivity of the first excursion probability can be estimated as:

$$\frac{\partial p_F(\boldsymbol{y})}{\partial y_q} \approx \frac{\partial \tilde{p}_F(\boldsymbol{y})}{\partial y_q} = \frac{1}{N}\sum_{j=1}^{N}\left(\frac{1}{\omega_{s_j}}\frac{\partial \tilde{p}_{s_j}\left(\boldsymbol{y}, \boldsymbol{z}^{\perp}_j\right)}{\partial y_q}\right). \tag{29}$$

Here, $\partial\tilde{p}_F(\boldsymbol{y})/\partial y_q$ is an estimate of $\partial p_F(\boldsymbol{y})/\partial y_q$ and $\partial\tilde{p}_{s_j}/\partial y_q$ denotes the derivative of the effective contribution with respect to the design parameter y_q, evaluated at $\boldsymbol{y}$ and $\boldsymbol{z}^{\perp}_j$. The notation for

s_j, $\boldsymbol{z}_j^{\perp}$, and ω_{s_j} is the same described in Equation (23). Therefore, the quantity $\partial\tilde{p}_{s_j}/\partial y_q$ can be calculated as:

$$\frac{\partial}{\partial y_q}\tilde{p}_{s_j}\left(\boldsymbol{y},\boldsymbol{z}_j^{\perp}\right)=\frac{\partial}{\partial y_q}\left(\int_{\Omega_j^{\parallel}(\boldsymbol{y})}\frac{1}{\sum_{h=1}^{n_\eta}\sum_{l=1}^{n_T}I_{F_{h,l}}\left(\boldsymbol{R}_{s_j}\boldsymbol{z}_j^{\perp}+\boldsymbol{\alpha}_{s_j}z_j^{\parallel}\right)}f_{Z_{s_j}^{\parallel}}(z_j^{\parallel})\,dz_j^{\parallel}\right). \tag{30}$$

Similarly to Equation (24), the integral in Equation (30) must be evaluated along the line l_j, a procedure explained later in Section 5.3. The integration domain $\Omega(\boldsymbol{y})$ defines the failure region corresponding to the design vector $\boldsymbol{y}$. Changes in $\boldsymbol{y}$ modify the geometry of this domain, and the resulting displacement of its boundaries is the sole source of sensitivity with respect to the design parameters. Therefore, Equation (29) defines the sensitivity of the first excursion probability estimator based on *multidomain Line Sampling*.

The coefficient of variation, $\delta_{\partial p_F/\partial y_q}$, associated with the sensitivity of the first excursion probability estimator in Equation (29), can be readily derived as follows:

$$\delta_{\partial\tilde{p}_F/\partial y_q}=\frac{1}{\partial\tilde{p}_F/\partial y_q}\sqrt{\frac{1}{N(N-1)}\sum_{j=1}^{N}\left(\left(\frac{1}{\omega_{s_j}}\frac{\partial\tilde{p}_{s_j}(\boldsymbol{y},\boldsymbol{z}_j^{\perp})}{\partial y_q}\right)-\frac{\partial\tilde{p}_F(\boldsymbol{y})}{\partial y_q}\right)^2} \tag{31}$$

where Equation (31) is evaluated under the assumption that $\partial p_F(\boldsymbol{y})/\partial y_q$ is nonzero.

Note that the estimator in Equation (30) evaluates exploration lines within $\Omega_j^{\parallel}(y)$ that are guided by the elementary failure domain F_j; as a consequence, the exploration line intersects the corresponding limit-state hyperplane of F_j orthogonally by construction, which is particularly informative for sensitivity estimation. In contrast, directional approaches such as DIS [37] and DDM [29] construct exploration lines as rays anchored at the origin and passing through a point associated with F_j, which can lead to less informative intersection angles and therefore require more simulations to achieve the same accuracy in the sensitivity estimates.

5. Practical Implementation

The implementation of Equations (24) and (30) requires special attention to four distinct aspects: the generation of samples $\boldsymbol{z}_j^{\perp}$, the calculation of relevant distances along the line l_j, the integration over the segment $\Omega_j^{\parallel}$, and the computation of partial derivatives of the relevant terms. These issues are addressed in this section.

5.1. Generation of Samples $\boldsymbol{z}_j^{\perp}$

The generation of independent and identically distributed samples $\boldsymbol{z}_j^{\perp},\ j = 1, \ldots, N$, which follow a $(n_{KL} - 1)$-dimensional standard multivariate Gaussian distribution, can be performed using the following procedure:

1. Define $I = \{(i, k) : i = 1, \ldots, n_\eta;\ k = 1, \ldots, n_T\}$ as the set of all index pairs. Each pair (i, k) can be mapped to a unique index in $\{1, \ldots, n_\eta n_T\}$.
2. For $j = 1, \ldots, N$, repeat Steps 2a–2c:
   (a) Select a pair (i, k) from I according to the weights $\omega_{i,k}$ in Equation (22), and let s_j denote the index corresponding to the selected pair.
   (b) Generate a sample $\boldsymbol{z}_j$ following an n_{KL}-dimensional standard Gaussian distribution.
   (c) Calculate [49, 51]:

$$\boldsymbol{R}_{s_j} \boldsymbol{z}_j^{\perp} = \boldsymbol{z}_j - \left(\boldsymbol{\alpha}_{s_j}^T \boldsymbol{z}_j\right) \boldsymbol{\alpha}_{s_j} \tag{32}$$

To illustrate how the algorithm works, Figure 6 presents a schematic representation for the case where $n_\eta = 1$ and $n_T = n_{KL} = 2$. Following Step 2a, the selected element is $s_1 = (1, 2)$, and, as specified in Step 2b, the corresponding sample $\boldsymbol{z}_1$ is generated and represented by a black dot in Figure 6. Then, in Step 2c, the sought quantity corresponds to $\boldsymbol{R}_{s_1} \boldsymbol{z}_1^{\perp}$, which is a vector represented with a dark blue arrow. This vector can be calculated by subtracting the vector $\left(\boldsymbol{\alpha}_{s_1}^T \boldsymbol{z}_1\right) \boldsymbol{\alpha}_{s_1}$, represented by a dark red arrow, from the original sample $\boldsymbol{z}_1$. This step is crucial for the multidomain Line Sampling implementation, as the quantity required by the method is $\boldsymbol{R}_{s_1} \boldsymbol{z}_1^{\perp}$, rather than just $\boldsymbol{z}_1^{\perp}$. This leads to a computational advantage, as it avoids explicitly computing the rotation matrices $\boldsymbol{R}_{s_1}$ for each sample.

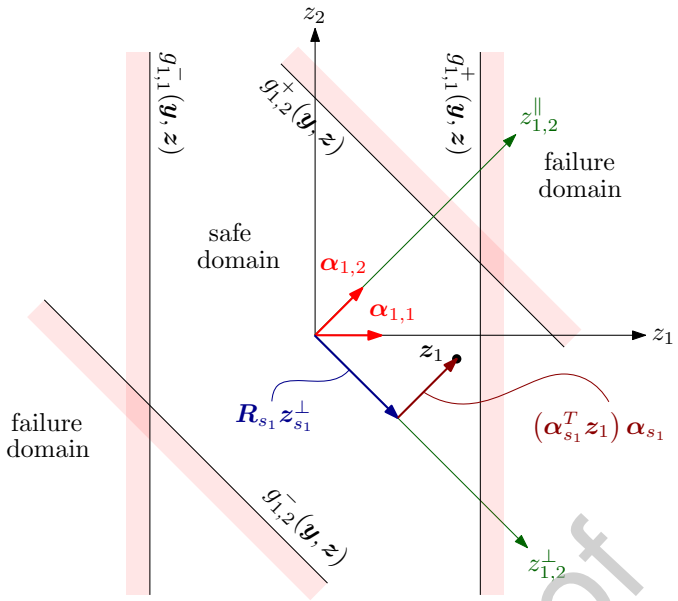

Figure 6: Representation of sample generation for the case where $n_\eta = 1$ and $n_T = n_{KL} = 2$.

5.2. Computation of Relevant Distances Along l_j

To address the line integration problem in Equations (24) and (30), it is important to recognize that, for a given realization of the sample $\boldsymbol{z}_j$, the integration domain $\Omega^{\parallel}_j(\boldsymbol{y})$ may exhibit varying degrees of overlap between elementary failure domains. Therefore, it is essential to geometrically identify the locations along the line l_j where the overlap between elementary failure domains changes. To precisely describe these locations, we use the rotated coordinate system introduced in Equation (19). Any point $\boldsymbol{z}$ in standard normal space can be written, in terms of the (i,k)-th rotated coordinate system, as $\boldsymbol{z} = \boldsymbol{R}_{i,k}\boldsymbol{z}^{\perp}_{i,k} + \boldsymbol{\alpha}_{i,k}c(\boldsymbol{y})$, where $c(\boldsymbol{y})$ represents how much one moves, positively or negatively, from the base point $\boldsymbol{R}_{i,k}\boldsymbol{z}^{\perp}_{i,k}$ along the axis defined by the important direction $\boldsymbol{\alpha}_{i,k}$. Consequently, the response of interest can be expressed as:

$$\eta_i\left(t_k, \boldsymbol{y}, \boldsymbol{R}_{i,k}\boldsymbol{z}^{\perp}_{i,k} + \boldsymbol{\alpha}_{i,k}c(\boldsymbol{y})\right) = \eta^{\perp}_i\left(t_k, \boldsymbol{y}, \boldsymbol{R}_{i,k}\boldsymbol{z}^{\perp}_{i,k}\right) + c(\boldsymbol{y}) \cdot \eta^{\parallel}_i\left(t_k, \boldsymbol{y}, \boldsymbol{\alpha}_{i,k}\right), \tag{33}$$

where $\eta^{\perp}_i$ is the perpendicular response of interest, and $\eta^{\parallel}_i$ is the unit parallel response of interest, both obtained by evaluating the Gaussian vector in Equation (7) at $\boldsymbol{R}_{i,k}\boldsymbol{z}^{\perp}_{i,k}$ and $\boldsymbol{\alpha}_{i,k}$, respectively. Then, the quantities $\eta^{\perp}_i$ and $\eta^{\parallel}_i$ are defined as:

$$\eta^{\perp}_i(t_k, \boldsymbol{y},\, \boldsymbol{R}_{i,k}\boldsymbol{z}^{\perp}_{i,k}) = \boldsymbol{a}_{i,k}(\boldsymbol{y})^T\, \boldsymbol{R}_{i,k}\boldsymbol{z}^{\perp}_{i,k}, \quad i = 1,\ldots,n_\eta,\ k = 1,\ldots,n_T, \tag{34}$$

$$\eta^{\parallel}_i(t_k, \boldsymbol{y},\, \boldsymbol{\alpha}_{i,k}) = \boldsymbol{a}_{i,k}(\boldsymbol{y})^T\, \boldsymbol{\alpha}_{i,k}, \quad i = 1,\ldots,n_\eta,\ k = 1,\ldots,n_T. \tag{35}$$

The quantity c, from Equation (33), plays a crucial role in evaluating the one-dimensional integral. To illustrate its geometric and physical meaning, Figure 7 presents the case where $n_\eta = 1$ and $n_T = n_{KL} = 2$, in the context of estimating the effective contribution $p_{1,2}$. For this case, a sample realization $\boldsymbol{z}_1^\perp$ has been generated, together with the corresponding line l_1 and the integration domain $\Omega_1^\parallel(\boldsymbol{y})$ depicted along this line. To proceed, it is necessary to explicitly define c at the points where the response of interest meets the positive and negative thresholds, for each elementary failure domain. Along each line l_j, the distances from the point $\boldsymbol{z}_j^\perp$ to the intersections with the corresponding hyperplanes, each defined by its own performance function, are called *crossing distances* and denoted by $c_{i,k}^{+,j}$ and $c_{i,k}^{-,j}$. The subscript (i,k) refers to the i-th response of interest at the k-th time instant, and the superscript j indicates the sample (and associated line) for which the distance is computed. In addition, the superscripts $(+)$ and $(-)$ indicate the distances to the positive (response η_i up-crossing its threshold b_i at time t_k) and negative (response η_i down-crossing its threshold b_i at time t_k) limit state functions, respectively. In Figure 7, the case corresponding to sample $j = 1$, with the pair of indices (i,k) given by $s_1 = (1,2)$, is presented. Therefore, for an arbitrary sample $\boldsymbol{z}_j^\perp$ with associated index s_j, evaluating Equation (33) at the points where the response equals the thresholds b_i and $-b_i$ at the time instant t_k along the line l_j, leads to:

$$b_i = \boldsymbol{a}_{i,k}(\boldsymbol{y})^T \boldsymbol{R}_{s_j} \boldsymbol{z}_j^\perp + c_{i,k}^{+,j}(\boldsymbol{y}) \cdot \boldsymbol{a}_{i,k}(\boldsymbol{y})^T \boldsymbol{\alpha}_{s_j} \tag{36}$$

$$-b_i = \boldsymbol{a}_{i,k}(\boldsymbol{y})^T \boldsymbol{R}_{s_j} \boldsymbol{z}_j^\perp + c_{i,k}^{-,j}(\boldsymbol{y}) \cdot \boldsymbol{a}_{i,k}(\boldsymbol{y})^T \boldsymbol{\alpha}_{s_j}. \tag{37}$$

Then, rewriting Equations (36) and (37) in terms of the perpendicular and unit parallel responses defined in Equations (34) and (35), the distances $c_{i,k}^{-,j}$ and $c_{i,k}^{+,j}$ associated with the line l_j are defined as:

$$c_{i,k}^{-,j} = \frac{-b_i - \eta_i^\perp(t_k,\, \boldsymbol{y},\, \boldsymbol{R}_{s_j}\boldsymbol{z}_j^\perp)}{\eta_i^\parallel(t_k,\, \boldsymbol{y},\, \boldsymbol{\alpha}_{s_j})}, \quad i = 1,\ldots,n_\eta,\ k = 1,\ldots,n_T,\ j = 1,\ldots,N, \tag{38}$$

$$c_{i,k}^{+,j} = \frac{b_i - \eta_i^\perp(t_k,\, \boldsymbol{y},\, \boldsymbol{R}_{s_j}\boldsymbol{z}_j^\perp)}{\eta_i^\parallel(t_k,\, \boldsymbol{y},\, \boldsymbol{\alpha}_{s_j})}, \quad i = 1,\ldots,n_\eta,\ k = 1,\ldots,n_T,\ j = 1,\ldots,N, \tag{39}$$

where it is assumed that the unit parallel response $\eta_i^\parallel(t_k, \boldsymbol{y}, \boldsymbol{\alpha}_{s_j})$ takes nonzero values. Therefore, Equations (38) and (39) provide a measure of how much it is necessary to amplify the unit parallel response $\eta_i^\parallel\left(t_k, \boldsymbol{y},\, \boldsymbol{\alpha}_{s_j}\right)$, given a perpendicular response $\eta_i^\perp\left(t_k, \boldsymbol{y},\, \boldsymbol{R}_{s_j}\boldsymbol{z}_j^\perp\right)$, in order to reach the

failure condition at the time instant t_k. It is important to note that the computation of the crossing distances requires performing two dynamic analyses: one for the perpendicular response and another for the unit parallel response (see Equations (34) and (35)).

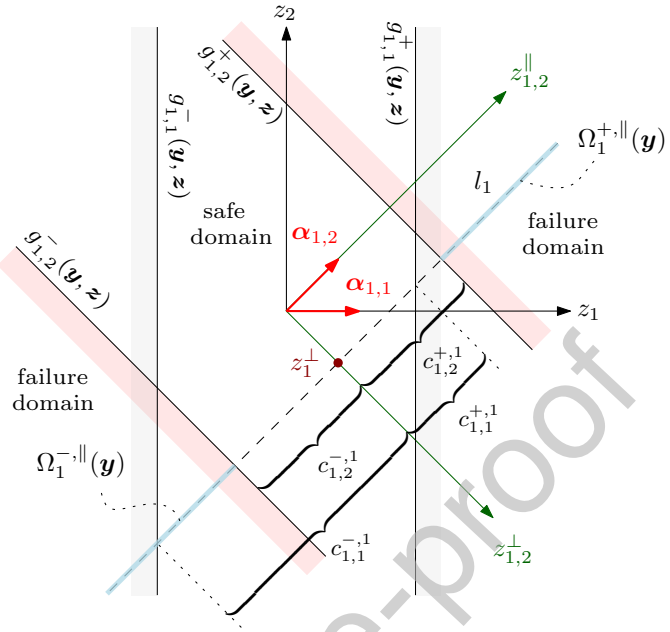

Figure 7: Crossing distances representation over line l_1 for the case where $n_\eta = 1$ and $n_T = n_{KL} = 2$.

5.3. One-dimensional Integration Over $\Omega^{\parallel}_j(\boldsymbol{y})$

5.3.1. Preliminary Notation

The estimation of the first excursion probability using multidomain Line Sampling requires the evaluation of the inner integral from Equation (20), for different realizations of $\boldsymbol{z}^{\perp}_j$, as shown in Equation (24). In order to clearly define the segments exhibiting different degrees of overlap between elementary failure domains over $\Omega^{\parallel}_j$, the distances $c^{-,j}_{i,k}$ and $c^{+,j}_{i,k}$, as defined in Equations (38) and (39), are grouped into the vector $\mathcal{C}^j$:

$$\mathcal{C}^j = \left\{ c^{-,j}_{i,k},\ c^{+,j}_{i,k} \right\}^T, \quad \text{for } i = 1,\ldots,n_\eta;\ k = 1,\ldots,n_T. \tag{40}$$

To facilitate integration implementation, the set is augmented with the endpoints $-\infty$ and $+\infty$, and its elements are sorted in ascending order to form the augmented vector:

$$\tilde{\mathcal{C}}^j_{\text{sort}} = \left\{ c^j_{[0]},\ c^j_{[1]},\ \ldots,\ c^j_{[n_F]},\ c^j_{[n_F+1]} \right\}^T, \tag{41}$$

where $n_F = 2n_\eta n_T$ denotes the total number of intersections between all limit state functions of

the elementary failure domains and the line l_j. The boundary values are set as $c^j_{[0]} = -\infty$ and $c^j_{[n_F+1]} = +\infty$, while the intermediate values $c^j_{[1]}, \ldots, c^j_{[n_F]}$ correspond to the sorted entries of $\mathcal{C}^j$ in ascending order. Each segment $[c^j_{[m-1]}, c^j_{[m]}]$, for $m = 1, \ldots, n_F + 1$, defines a segment of the line l_j where the number of overlapping elementary failure domains remains constant.

To track how the overlap between elementary failure domains changes between two consecutive segments, we define the vector $\mathcal{V}^j$, whose entries, $\nu^{-,j}_{i,k}$ and $\nu^{+,j}_{i,k}$, are called *transition indicators*:

$$\mathcal{V}^j = \left\{ \nu^{-,j}_{i,k} = -1,\ \nu^{+,j}_{i,k} = +1 \right\}^T, \quad \text{for } i = 1, \ldots, n_\eta;\ k = 1, \ldots, n_T, \tag{42}$$

where each element in $\mathcal{V}^j$ is associated with a corresponding distance in $\mathcal{C}^j$. The value $+1$ is assigned to each $\nu^{+,j}_{i,k}$ and -1 to each $\nu^{-,j}_{i,k}$. These values indicate whether an elementary failure domain becomes active $(+1)$ or inactive (-1) when traversing the line l_j in the direction of the important direction $\boldsymbol{\alpha}_{s_j}$. To align the transition indicators with the sorted vector $\tilde{\mathcal{C}}^j_{\text{sort}}$, a corresponding sorted transition indicator vector $\tilde{\mathcal{V}}^j_{\text{sort}}$ is introduced. This vector is constructed by applying the same permutation used to sort $\mathcal{C}^j$ to the elements of $\mathcal{V}^j$, and is extended by including two auxiliary entries at the boundaries. Specifically,

$$\tilde{\mathcal{V}}^j_{\text{sort}} = \left\{ \nu^j_{[0]},\ \nu^j_{[1]},\ \ldots,\ \nu^j_{[n_F]},\ \nu^j_{[n_F+1]} \right\}^T, \tag{43}$$

where the first and last elements are auxiliary values defined as $\nu^j_{[0]} = 0$ and $\nu^j_{[n_F+1]} = 0$, included to match the structure of $\tilde{\mathcal{C}}^j_{\text{sort}}$ in order to simplify the numerical implementation. This vector allows computing the number of active elementary failure domains in each segment $[c^j_{[m-1]},\ c^j_{[m]}]$ via a cumulative sum over $\nu^j_{[1]}$ to $\nu^j_{[m-1]}$, for $m = 1, \ldots, n_F + 1$, as explained later in this section.

5.3.2. Definition of the Integration Domain

To define the integration domain $\Omega^{\parallel}_j$, recall that integration is performed only within the failure domain F_{s_j} associated with the effective contribution being estimated, p_{s_j}; that is, in the intervals $(-\infty, -\beta_{s_j}] \cup [\beta_{s_j}, +\infty)$ within the line l_j. Let λ^j_N and λ^j_P denote the indices in the sorted vector $\tilde{\mathcal{C}}^j_{\text{sort}}$ such that:

$$c^j_{[\lambda^j_N]} = -\beta_{s_j}, \quad c^j_{[\lambda^j_P]} = \beta_{s_j}. \tag{44}$$

These correspond to the positions in the sorted vector $\tilde{\mathcal{C}}^j_{\text{sort}}$ that contain the negative and positive crossing distances associated with F_{s_j}. Note that the positive and negative portions of $\Omega^{\parallel}_j$ can also

be expressed in terms of segments as:

$$\Omega_j^{-,\parallel} = \bigcup_{r=1}^{\lambda_N^j} [c_{[r-1]}^j,\ c_{[r]}^j], \quad \Omega_j^{+,\parallel} = \bigcup_{r=\lambda_P^j+1}^{n_F+1} [c_{[r-1]}^j,\ c_{[r]}^j]. \tag{45}$$

The vectors defined in Equations (41) and (43) are illustrated in Figure 8 and Table 1 in the context of estimating the effective contribution $p_{1,1}$, where $n_\eta = 1$ and $n_T = n_{KL} = 2$. Three different samples along the coordinate $z_{1,1}^\perp$ are generated to demonstrate how the introduced vectors can retain useful information irrespective of the sample locations and/or the degree of overlap between elementary failure domains. The lines l_1, l_2, and l_3 are defined from the samples $z_1^\perp$, $z_2^\perp$, and $z_3^\perp$, respectively. The domains to be integrated correspond to the positive and negative portions of $\Omega_1^\parallel$, $\Omega_2^\parallel$, and $\Omega_3^\parallel$, represented by the light blue lines in the figure, where the sorted crossing distances in $\tilde{\mathcal{C}}_{\text{sort}}^j$ for each l_j are also labeled. The table compiles all corresponding numerical values, including the crossing distances in $\tilde{\mathcal{C}}_{\text{sort}}^j$ and $\mathcal{C}^j$, the transition indicators in $\tilde{\mathcal{V}}_{\text{sort}}^j$ with their associated entries in $\mathcal{V}^j$, and the positions λ_N^j and λ_P^j for each line. A detailed description of the figure is essential to highlight the challenges that may arise during the implementation of the method. For lines l_1 and l_3, the samples are generated inside an elementary failure domain, resulting in three distances being negative and three being positive, respectively. For line l_1, and similarly for l_2, the number of active elementary failure domains, following the important direction $\alpha_{1,1}$, first decreases, and then, increases, as shown by the values in $\tilde{\mathcal{V}}_{\text{sort}}^j$. In contrast, for line l_3, the pattern differs, as it remains inside at least one elementary failure domain for its entire length. It is also worth noting that, in the context of estimating $p_{1,1}$, the positions of λ_N^j and λ_P^j can vary significantly when exploring different lines l_j. This behavior, although seemingly complex to assess even in a two-dimensional example, can be readily organized using the quantities shown in Table 1.

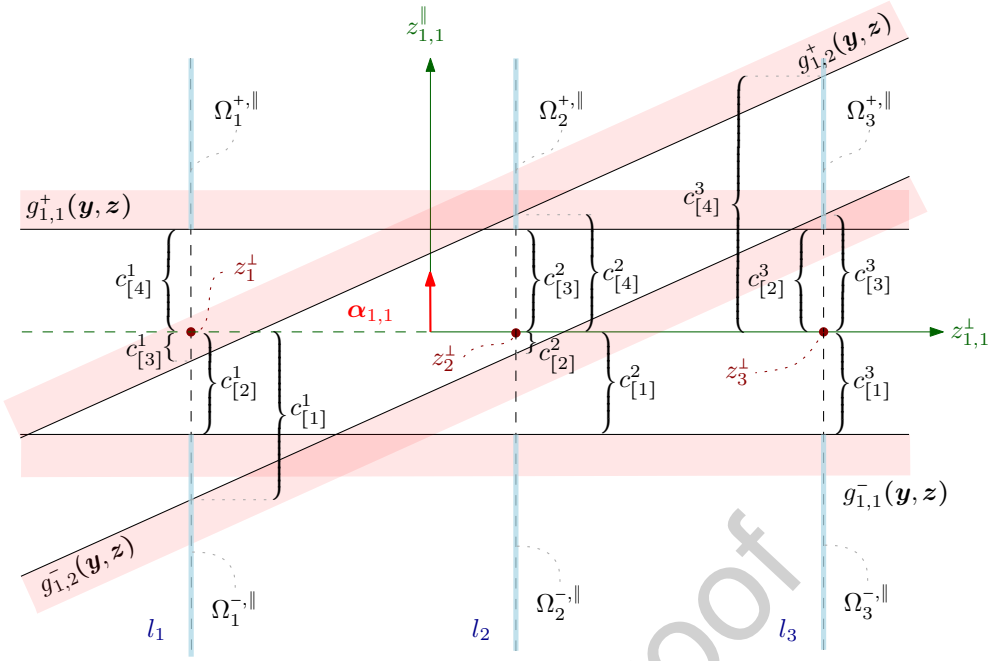

Figure 8: Schematic representation for estimating the effective contribution $p_{1,1}$, for the case where $n_\eta = 1$ and $n_T = n_{KL} = 2$, using three different samples.

Table 1: Values of the vectors $\mathcal{C}^j$, $\tilde{\mathcal{C}}^j_{\text{sort}}$, $\mathcal{V}^j$ and $\tilde{\mathcal{V}}^j_{\text{sort}}$ associated with the example presented in Figure 8.

line l_j	entry in $\mathcal{C}^j$	entry in $\tilde{\mathcal{C}}^j_{\text{sort}}$	entry in $\mathcal{V}^j$	entry in $\tilde{\mathcal{V}}^j_{\text{sort}}$	remarks
l_1	$c^{-,1}_{1,2}$	$c^1_{[1]}$	$\nu^{-,1}_{1,2}$	$\nu^1_{[1]} = -1$	
	$c^{-,1}_{1,1}$	$c^1_{[2]}$	$\nu^{-,1}_{1,1}$	$\nu^1_{[2]} = -1$	position λ^1_N
	$c^{+,1}_{1,2}$	$c^1_{[3]}$	$\nu^{+,1}_{1,2}$	$\nu^1_{[3]} = +1$	
	$c^{+,1}_{1,1}$	$c^1_{[4]}$	$\nu^{+,1}_{1,1}$	$\nu^1_{[4]} = +1$	position λ^1_P
l_2	$c^{-,2}_{1,1}$	$c^2_{[1]}$	$\nu^{-,2}_{1,1}$	$\nu^2_{[1]} = -1$	position λ^2_N
	$c^{-,2}_{1,2}$	$c^2_{[2]}$	$\nu^{-,2}_{1,2}$	$\nu^2_{[2]} = -1$	
	$c^{+,2}_{1,1}$	$c^2_{[3]}$	$\nu^{+,2}_{1,1}$	$\nu^2_{[3]} = +1$	position λ^2_P
	$c^{+,2}_{1,2}$	$c^2_{[4]}$	$\nu^{+,2}_{1,2}$	$\nu^2_{[4]} = +1$	
l_3	$c^{-,3}_{1,1}$	$c^3_{[1]}$	$\nu^{-,3}_{1,1}$	$\nu^3_{[1]} = -1$	position λ^3_N
	$c^{+,3}_{1,1}$	$c^3_{[2]}$	$\nu^{+,3}_{1,1}$	$\nu^3_{[2]} = +1$	position λ^3_P
	$c^{-,3}_{1,2}$	$c^3_{[3]}$	$\nu^{-,3}_{1,2}$	$\nu^3_{[3]} = -1$	
	$c^{+,3}_{1,2}$	$c^3_{[4]}$	$\nu^{+,3}_{1,2}$	$\nu^3_{[4]} = +1$	

5.3.3. Overlap of Elementary Failure Domains

The definition of the *overlap count* vector is introduced to compute the number of overlapping

elementary failure domains per segment, defined as:

$$\boldsymbol{m}^j = \left\{ m_1^j, \ldots, m_{n_S}^j \right\}^T, \quad n_S = n_F + 1, \tag{46}$$

where n_S corresponds to the number of segments within the line l_j, and m_r^j is defined as:

$$m_r^j = \begin{cases} m_r^{j,n}, & r = 1, \ldots, \lambda_N^j, \\ m_0, & r = \lambda_N^j + 1, \ldots, \lambda_P^j, \\ m_r^{j,p}, & r = \lambda_P^j + 1, \ldots, n_S, \end{cases} \tag{47}$$

where each $m_r^{j,n}$ and $m_r^{j,p}$ represents the number of active elementary failure domains within the r-th integration segment of $\Omega_j^{-,\|}(\boldsymbol{y})$ and $\Omega_j^{+,\|}(\boldsymbol{y})$, respectively, and m_0 is an integer number different from zero to facilitate the numerical implementation. These are computed recursively by accumulating the transition indicators $\nu_{[h]}^j$ across the segments, as follows:

$$m_r^{j,n} = n_\eta n_T + 1 + \sum_{h=1}^{r} \nu_{[h]}^j, \qquad r = 1, \ldots, \lambda_N^j, \tag{48}$$

$$m_r^{j,p} = n_\eta n_T + \sum_{h=1}^{r} \nu_{[h]}^j, \qquad r = \lambda_P^j + 1, \ldots, n_S, \tag{49}$$

where the $+1$ term in Equation (48) ensures that the first segment starts with $n_\eta n_T$ elementary failure domains active. This term is not required in Equation (49) due to the way the transition indicators are defined. The elements in $\boldsymbol{m}^j$ determine the denominator used in the integrand of Equation (24). Intermediate segments between λ_N^j and λ_P^j are represented by m_0 even if they contain elementary failure domains, since they do not contribute to the integration domain $\Omega_j^{\|}(\boldsymbol{y})$. These segments can be identified by introducing a boolean *selector vector* $\boldsymbol{\kappa}^j = \{\kappa_r^j, \ldots, \kappa_{n_S}^j\}^T \in \{0, 1\}$ with $r = 1, \ldots, n_S$, yielding a vector of dimensions $n_S \times 1$, defined as:

$$\kappa_r^j = \begin{cases} 1, & r \in \{1, \ldots, \lambda_N^j\} \cup \{\lambda_P^j + 1, \ldots, n_S\}, \\ 0, & \text{otherwise}, \end{cases} \tag{50}$$

which indicates the segments that contribute to the integration over $\Omega_j^{\|}$. Figure 9 illustrates the values of the overlap count vector $\boldsymbol{m}^j$ for the three lines of the example in Figure 8. The values

shown correspond to integration segments where the selector vector satisfies $\kappa_r^j = 1$. It is worth noting that, for all lines, the first and last integration segments have an overlap count of $n_\eta n_T = 2$. For lines l_1 and l_2, there are three valid integration segments, while for line l_3 there are four. In addition, it is straightforward to note that the number of negative and positive segments varies for each line.

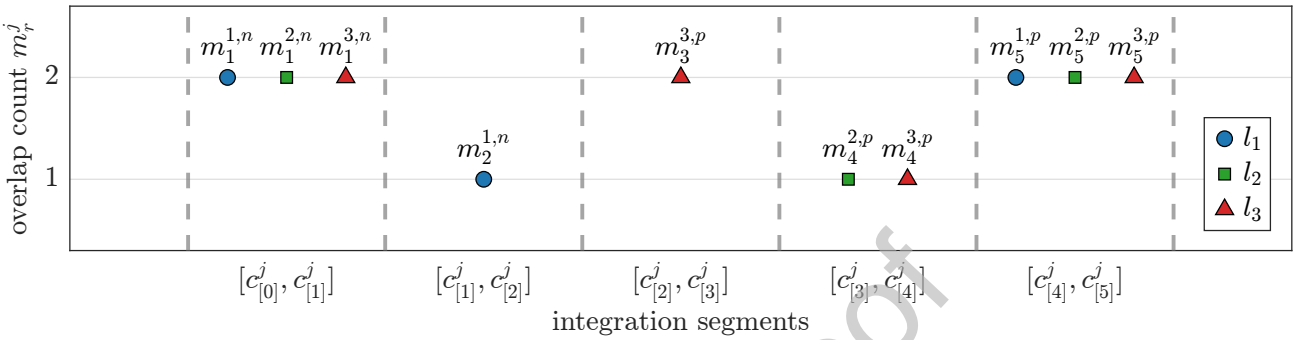

Figure 9: Overlap count vector calculation for the example presented in Figure 8.

5.4. Estimation of the Effective Contribution and Its Sensitivity

The application of the previous definitions leads to a more compact expression for the estimation of the effective contribution $\tilde{p}_{s_j}(\boldsymbol{y})$ shown in Equation (24), expressed as:

$$\tilde{p}_{s_j}(\boldsymbol{y}) = \sum_{r=1}^{n_S} \frac{\kappa_r^j}{m_r^j} \left(\Phi\left(c_{[r]}^j\right) - \Phi\left(c_{[r-1]}^j\right) \right). \tag{51}$$

Analogously, the derivative of the estimation of the effective contribution with respect to the design parameter y_q, based on Equation (30), becomes:

$$\frac{\partial}{\partial y_q}\left(\tilde{p}_{s_j}(\boldsymbol{y})\right) = \sum_{r=1}^{n_S} \frac{\kappa_r^j}{m_r^j} \left(\phi\left(c_{[r]}^j\right) \frac{\partial c_{[r]}^j}{\partial y_q} - \phi\left(c_{[r-1]}^j\right) \frac{\partial c_{[r-1]}^j}{\partial y_q} \right), \tag{52}$$

where $\partial c_{[r]}^j / \partial y_q$ denotes the partial derivative of the distance $c_{[r]}^j$ with respect to the design parameter y_q, the calculation of which is detailed in Section 5.5. It is important to highlight that with the convention $m_r^j = m_0$ whenever $\kappa_r^j = 0$, all the denominators in Equations (51) and (52) remain nonzero. For completeness, Appendix C provides a detailed derivation of Equation (52) from Equation (30). It is noted that, under the adopted formulation, Equation (52) can also be obtained by direct differentiation of Equation (51).

The estimation of the effective contribution and its derivative, using Equations (51) and (52), allows for the computation of the first excursion probability via Equation (24), and its sensitivity

via Equation (30). For a given exploration line l_j, both estimators can be evaluated simultaneously. This constitutes a significant advantage, as the sensitivity estimation becomes a byproduct of the first excursion probability estimation.

5.5. Partial Derivatives

The sensitivity of the first excursion probability with respect to a design parameter, as shown in Equation (29), depends on the partial derivative of the effective contribution of the failure probability with respect to that parameter. According to Leibniz's rule [52] and Equation (52), this quantity also depends on the partial derivative of the crossing distance with respect to the same design parameter. This partial derivative can be obtained by directly differentiating Equation (38) and (39) with respect to the design parameter y_q:

$$\frac{\partial c_{i,k}^{-,j}(\boldsymbol{y})}{\partial y_q} = \frac{-\dfrac{\partial \boldsymbol{a}_{i,k}(\boldsymbol{y})}{\partial y_q}^T \boldsymbol{R}_{s_j} \boldsymbol{z}_j^{\perp} \; - \; c_{i,k}^{-,j} \dfrac{\partial \boldsymbol{a}_{i,k}(\boldsymbol{y})}{\partial y_q}^T \boldsymbol{\alpha}_{s_j}}{\eta_i^{\parallel}(t_k,\, \boldsymbol{y},\, \boldsymbol{\alpha}_{s_j})}, \tag{53}$$

$$\frac{\partial c_{i,k}^{+,j}(\boldsymbol{y})}{\partial y_q} = \frac{-\dfrac{\partial \boldsymbol{a}_{i,k}(\boldsymbol{y})}{\partial y_q}^T \boldsymbol{R}_{s_j} \boldsymbol{z}_j^{\perp} \; - \; c_{i,k}^{+,j} \dfrac{\partial \boldsymbol{a}_{i,k}(\boldsymbol{y})}{\partial y_q}^T \boldsymbol{\alpha}_{s_j}}{\eta_i^{\parallel}(t_k,\, \boldsymbol{y},\, \boldsymbol{\alpha}_{s_j})}, \tag{54}$$

where $\partial \boldsymbol{a}_{i,k}(\boldsymbol{y})^T / \partial y_q$ denotes the derivative of the vector $\boldsymbol{a}_{i,k}(\boldsymbol{y})$ with respect to the parameter y_q. Evaluating Equation (53) or (54) is equivalent to performing two sensitivity analyses. In practice, for a given line l_j, these analyses are in addition to the two dynamic analyses required, as shown in Section 5.2. In order to facilitate the implementation, the derivatives $\partial c_{i,k}^{-,j} / \partial y_q$ and $\partial c_{i,k}^{+,j} / \partial y_q$, as obtained from Equations (53) and (54), are grouped into the vector $\mathcal{D}^j$:

$$\mathcal{D}^j = \left\{ \frac{\partial c_{i,k}^{-,j}}{\partial y_q},\; \frac{\partial c_{i,k}^{+,j}}{\partial y_q} \right\}^T, \quad \text{for } i = 1, \ldots, n_\eta;\; k = 1, \ldots, n_T. \tag{55}$$

Following the same ordering applied to $\mathcal{C}^j$, the elements of $\mathcal{D}^j$ are rearranged to form the sorted derivative vector:

$$\tilde{\mathcal{D}}_{\text{sort}}^j = \left\{ \frac{\partial c_{[0]}^j}{\partial y_q},\; \frac{\partial c_{[1]}^j}{\partial y_q},\; \ldots,\; \frac{\partial c_{[n_F]}^j}{\partial y_q},\; \frac{\partial c_{[n_F+1]}^j}{\partial y_q} \right\}^T. \tag{56}$$

The vector $\boldsymbol{a}_{i,k}(\boldsymbol{y})$, defined in Section 2.2, depends on the i-th unit impulse response function $h_i(t, \boldsymbol{y})$. Its derivative can be obtained by directly differentiating Equation (6), resulting in:

$$\frac{\partial \boldsymbol{a}_{i,k}(\boldsymbol{y})}{\partial y_q} = \sum_{m=1}^{k} \Delta t \epsilon_m \frac{\partial h_i\left(t_k - t_m, \boldsymbol{y}\right)}{\partial y_q} \boldsymbol{\psi}_m, \tag{57}$$

where $\partial h_i\left(t, \boldsymbol{y}\right)/\partial y_q$ is the partial derivative of the i-th unit impulse response function with respect to the design parameter y_q. The unit impulse response in Equation (6) is determined by the mass and damping matrices, the coupling vector, and the spectral properties of the system. Accordingly, its partial derivative with respect to a design parameter is computed via the chain rule, as described in Appendix D. It is important to note that, in this work, the partial derivatives of the eigenvectors and eigenvalues are computed using the method proposed in [39].

5.6. Summary

The first excursion probability and its sensitivity with respect to a design parameter, using multidomain Line Sampling applied to a linear system subjected to Gaussian loading, can be calculated as follows:

1. Model the Gaussian loading $\boldsymbol{p}$ using the Karhunen-Loève expansion (see Equation (1)).
2. Specify the mass, damping, and stiffness matrices $\boldsymbol{M}$, $\boldsymbol{C}$, and $\boldsymbol{K}$, the design parameter vector $\boldsymbol{y}$, and the response thresholds $\boldsymbol{b}$ (see Equation (2)).
3. Assemble the augmented matrices $[\boldsymbol{M}_a]$, $[\boldsymbol{K}_a]$, and the vector $\{\boldsymbol{g}_a\}$ (see Equations (3) and (4)).
4. Compute the vectors $\boldsymbol{a}_{i,k}(\boldsymbol{y})$ and their derivatives $\partial \boldsymbol{a}_{i,k}(\boldsymbol{y})/\partial y_q$ (see Equations (6) and (57)).
5. Multidomain Line Sampling loop for $j = 1, \ldots, N$:
   (a) Generate a sample $\boldsymbol{z}_j^{\perp}$ in the orthogonal space and define the associated line l_j (see Section 5.1).
   (b) For the line l_j, compute distances $c_{i,k}^{-,j}$ and $c_{i,k}^{+,j}$ (see Equations (38) and (39)) and build the vector $\mathcal{C}^j$ (see Equation (40)). Analogously, compute the transition indicators $\nu_{i,k}^{-,j}$ and $\nu_{i,k}^{+,j}$ and build the vector $\mathcal{V}^j$ (see Equation (42)).
   (c) Build the sorted vectors $\tilde{\mathcal{C}}_{\text{sort}}^j$ and $\tilde{\mathcal{V}}_{\text{sort}}^j$ (see Equations (41) and (43)).
   (d) Identify the negative and positive indices λ_N^j and λ_P^j (Equation (44)).
   (e) For the line l_j, compute the derivative of the distances $\partial c_{i,k}^{-,j}/\partial y_q$ and $\partial c_{i,k}^{+,j}/\partial y_q$ (see Equations (53) and (54)) and build the vectors $\mathcal{D}^j$ (see Equation (55)) and $\tilde{\mathcal{D}}_{\text{sort}}^j$ (see Equation (56)).

(f) Build the overlap count vector $\boldsymbol{m}^j$ and the selector boolean vector $\boldsymbol{\kappa}^j$ (see Equations (48), (49) and (50)).

(g) Evaluate the effective contribution $\tilde{p}_{s_j}(\boldsymbol{y})$ (see Equation (51)) and its derivative $\partial\left(\tilde{p}_{s_j}(\boldsymbol{y})\right)/\partial y_q$ (see Equation (52)).

6. Compute the first excursion probability estimator $\tilde{p}_F(\boldsymbol{y})$ (Equation (23)) and its sensitivity $\partial\tilde{p}_F(\boldsymbol{y})/\partial y_q$ (Equation (29)) by averaging the contributions over all N lines.

To facilitate numerical implementation, the steps described above are also provided in pseudo-code form, as shown in Appendix E.

6. Examples

6.1. Overview of the examples

This section showcases the application of multidomain Line Sampling to two different problems. The first example involves a quarter-car model represented by a two-degree-of-freedom system with non-proportional damping. The second example involves a large-scale finite element model of a 16-story building assuming proportional damping. The results are analyzed and compared with existing methods in the literature to demonstrate the efficiency of the proposed method.

All numerical simulations were performed in MATLAB R2023a on a laptop equipped with an Intel® Core™ i9–12900H processor (20 cores, up to 4.9 GHz) and 32 GB RAM, running Windows 11 (64-bit). All computations were executed on the CPU.

6.2. Example 1: Quarter-car model

The first example is an idealization of a car's suspension, modeled as a two-degree-of-freedom system and commonly referred to as a quarter-car model, as shown in Figure 11. This model is based on an example presented in [53]. The behavior of the system is governed by the following pair of ordinary differential equations:

$$\begin{bmatrix} m_1 & 0 \\ 0 & m_2 \end{bmatrix} \begin{Bmatrix} \ddot{x}_1(t,\boldsymbol{y},\boldsymbol{z}) \\ \ddot{x}_2(t,\boldsymbol{y},\boldsymbol{z}) \end{Bmatrix} + \begin{bmatrix} c_1+c_2 & -c_2 \\ -c_2 & c_2 \end{bmatrix} \begin{Bmatrix} \dot{x}_1(t,\boldsymbol{y},\boldsymbol{z}) \\ \dot{x}_2(t,\boldsymbol{y},\boldsymbol{z}) \end{Bmatrix} + \begin{bmatrix} k_1+k_2 & -k_2 \\ -k_2 & k_2 \end{bmatrix} \begin{Bmatrix} x_1(t,\boldsymbol{y},\boldsymbol{z}) \\ x_2(t,\boldsymbol{y},\boldsymbol{z}) \end{Bmatrix} = \begin{Bmatrix} k_1 w(t) + c_1 \dot{w}(t) \\ 0 \end{Bmatrix}, \tag{58}$$

where the unsprung and sprung masses of the car are $m_1 = 15$ kg and $m_2 = 290$ kg, respectively. The tire stiffness is $k_1 = 191000$ N/m, and the suspension stiffness is $k_2 = 16200$ N/m. In addition, the non-proportional damping matrix is composed of the tire damping coefficient $c_1 = 100$ Ns/m and the suspension damping coefficient $c_2 = 2500$ Ns/m.

The road profile $w(t, \boldsymbol{z})$ serves as the load input for the model. It is modeled as a zero-mean stationary Gaussian random field with a squared exponential covariance kernel, a correlation length of 3 m, and a standard deviation of 0.01 m. The car is assumed to travel at 25 m/s over a distance of 125 m. The road profile is discretized into 1001 equidistant points, corresponding to a total of $n_{KL} = 1001$ terms, which results in 1001 elementary failure domains. The expansion is not truncated, since the aim here is to illustrate the performance of the proposed sensitivity analysis. Time is discretized into intervals of $\Delta t = 0.005$ s, for a total duration of 5 s.

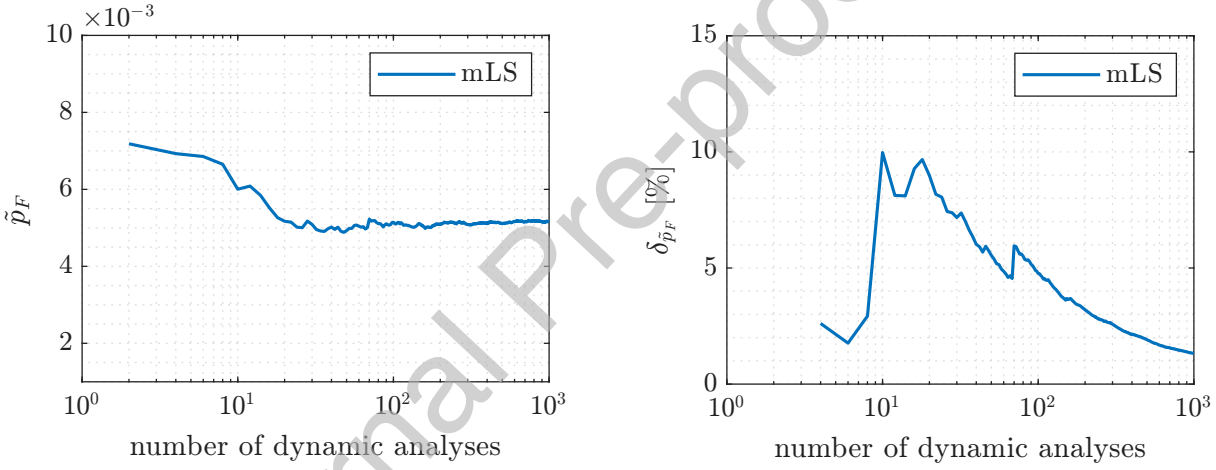

(a) Evolution of the first excursion probability estimator with respect to the number of dynamic analyses.

(b) Coefficient of variation of the first excursion probability estimator with respect to the number of dynamic analyses.

Figure 10: **Example 1**: Evolution of the first excursion probability estimator using multidomain Line Sampling (mLS).

The car's suspension design is paramount to fulfilling comfort requirements while driving over a road profile. Two key response variables can be used to assess this: the acceleration of the sprung mass and the suspension stroke, defined as the relative displacement between the sprung and unsprung masses. In this example, the latter is considered, and the response of interest is the displacement of mass m_2 with respect to mass m_1, expressed as $\eta(t, \boldsymbol{y}, \boldsymbol{z}) = |x_2(t, \boldsymbol{y}, \boldsymbol{z}) - x_1(t, \boldsymbol{y}, \boldsymbol{z})|$. The threshold level associated with the response of interest is set to $b = 3.5 \times 10^{-2}$ m. The first excursion probability for the problem is estimated using mLS, which gives $\tilde{p}_F = 5.1 \times 10^{-3}$, as shown in Figure 10a. Furthermore and as observed from Figure 10b, the coefficient of variation

of the probability estimator is quite low, as it never exceeds 10%.

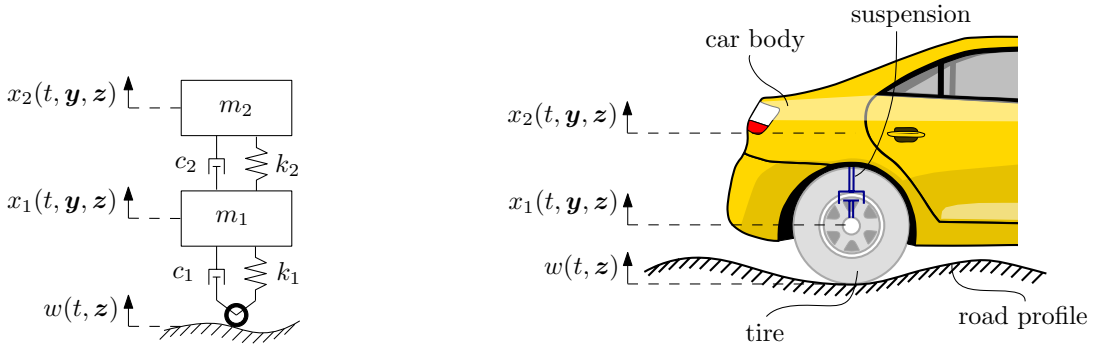

(a) 2-degree-of-freedom representation.

(b) Physical representation.

Figure 11: **Example 1:** Quarter-car model.

The objective is to estimate the sensitivity of the first excursion probability using mLS with respect to the design vector $\mathbf{y} = [y_1, y_2]^T$, where $y_1 = m_2$ and $y_2 = k_2$, and to establish a comparison with DIS [8] and DDM [29]. The comparison is based on the number of dynamic analyses required to obtain a single estimate of the sensitivity and its corresponding coefficient of variation. It is important to note that mLS requires two dynamic analyses and two sensitivity analyses per simulation, while DIS and DDM require one dynamic analysis and one sensitivity analysis.

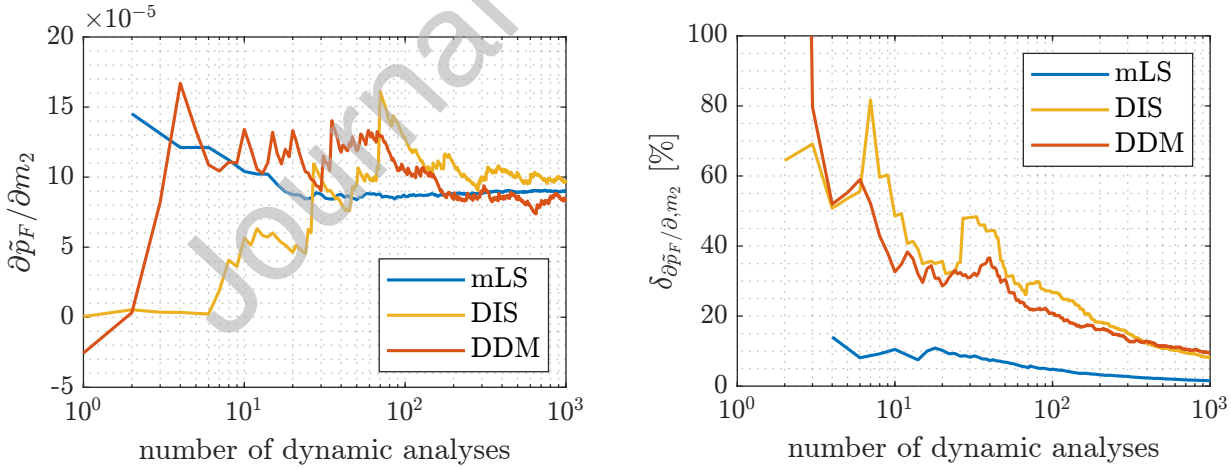

(a) Evolution of the sensitivity estimator with respect to the number of dynamic analyses.

(b) Coefficient of variation of the sensitivity estimator with respect to the number of dynamic analyses.

Figure 12: **Example 1:** Comparison of sensitivity results associated with m_2 using Directional Importance Sampling (DIS), the Domain Decomposition Method (DDM), and multidomain Line Sampling (mLS).

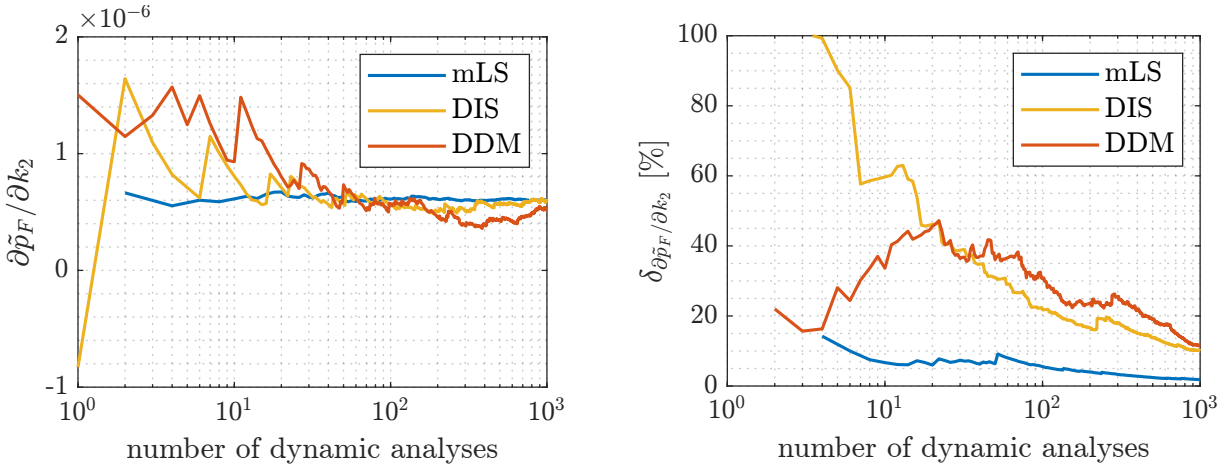

(a) Evolution of the sensitivity estimator with respect to the number of dynamic analyses.

(b) Coefficient of variation of the sensitivity estimator with respect to the number of dynamic analyses.

Figure 13: **Example 1:** Comparison of sensitivity results associated with k_2 using Directional Importance Sampling (DIS), the Domain Decomposition Method (DDM), and multidomain Line Sampling (mLS).

The evolution of the sensitivity estimators associated with m_2 and k_2 is presented in Figures 12 and 13, respectively, in terms of the number of dynamic analyses performed per simulation. A total of 1×10^3 dynamic analyses is considered in this example. For the design parameter m_2, Figure 12a shows that all methods converge to a similar value for the sensitivity estimator, with the mLS estimator exhibiting remarkably stable behavior. This is confirmed in Figure 12b, where the coefficients of variation of the DDM and DIS estimators reach approximately 10% with 1×10^3 dynamic analyses, whereas the mLS estimator achieves the same level with only 20 dynamic analyses. Similarly, for the second parameter k_2, the sensitivity estimator computed using mLS achieves a coefficient of variation of 10% after just 50 dynamic analyses, whereas the other methods again require approximately 1×10^3 dynamic analyses. Note that the discrepancies between the results at smaller numbers of dynamic analyses are purely due to random sampling variability, not to bias. All methods yield unbiased estimators, which converge as more dynamic analyses are accumulated. It is worth noting that, in Figures 12 and 13, the coefficients of variation obtained with mLS are significantly smaller than those of DIS and DDM and exhibit only a mild decrease with the number of dynamic analyses. This behavior is a direct consequence of the way mLS explores the failure domain: each exploration line typically intersects the elementary failure domain (associated with the effective contribution being estimated) perpendicular to their boundary, thereby capturing more relevant sensitivity information. In contrast, the directional approaches (DIS and DDM) explore the failure domain using lines anchored at the origin, so that, when these lines intersect the elementary failure domains, the effect of parameter perturbations

is less pronounced and is therefore captured less efficiently in the sensitivity estimates.

In Table 2, the computational effort of the different methods is compared using the speed-up factor $\boldsymbol{S}_u$, which quantifies the efficiency gains of the proposed technique. The speed-up factor is computed as the ratio between the number of dynamic analyses $\mathrm{N}^{(q)}$ required by the reference method and that required by mLS for each parameter y_q, to reach a coefficient of variation of 10%. The last column presents the mean number of required dynamic analyses for estimating one sensitivity, given by $\mathrm{N}_{\mathrm{mean}} = (\sum_{q=1}^{n_Y} \mathrm{N}^{(q)})/n_Y$. For the sensitivity with respect to m_2, mLS achieves a speed-up of 32.0 over DIS and 43.0 over DDM. Similarly, for k_2, the respective speed-up factors are 19.9 and 30.7. These results confirm that mLS substantially reduces the computational effort required, while preserving the accuracy of the sensitivity estimates. A similar behavior is observed when considering the average computational cost, where mLS achieves a speed-up of 23.33 over DIS and 34.21 over DDM based on the mean number of dynamic analyses.

Method	$\partial\tilde{p}_F/\partial m_2$	$\mathrm{N}^{(1)}$	$\partial\tilde{p}_F/\partial k_2$	$\mathrm{N}^{(2)}$	$\mathbf{N}_{\mathrm{mean}}$
mLS	8.75×10^{-5}	20	6.29×10^{-7}	50	**35.00**
DIS	1.03×10^{-4}	640	5.99×10^{-7}	993	**816.50**
DDM	8.82×10^{-5}	859	6.05×10^{-7}	1536	**1197.50**
$\boldsymbol{S}_u$ (mLS vs DIS)	**32.00**		**19.86**		**23.33**
$\boldsymbol{S}_u$ (mLS vs DDM)	**42.95**		**30.72**		**34.21**

Table 2: **Example 1:** Comparison of sensitivity estimates, number of dynamic analyses ($\mathrm{N}^{(q)}$), and speed-up ($\boldsymbol{S}_u$) of mLS versus other methods, for a target coefficient of variation of 10%.

Furthermore, the results were validated against finite difference (FD) estimates. For the estimation, a central-difference scheme is used with a total of 2×10^6 independent directional sampling samples (split equally between forward and backward steps), applying a relative perturbation of $\Delta_i = 0.01\, y_i$ to each parameter. The same random seeds were used in the forward and backward simulations in order to reduce estimator variance. Table 3 presents the comparison, where the proposed method achieves a coefficient of variation of 1%, revealing excellent agreement between the sensitivity estimates obtained using mLS and FD.

Method	$\partial\tilde{p}_F/\partial m_2$	$\partial\tilde{p}_F/\partial k_2$
mLS	8.80×10^{-5}	6.14×10^{-7}
FD	8.96×10^{-5}	6.25×10^{-7}

Table 3: Comparison of sensitivity estimates using mLS and FD.

To further examine the numerical behavior of the estimator, we investigate how the computational effort required for estimating the sensitivities with respect to the sprung mass m_2 and the suspension stiffness k_2 depends on the magnitude of the first-excursion probability. For each estimator, Figure 14 shows the mean number of dynamic analyses required by mLS to reach a coefficient of variation of 5%. At each probability level, this mean is computed over 500 independent simulations. Different failure probabilities are generated by varying the response threshold in uniform steps, covering $p_F \in [10^{-7}, 10^{-1}]$. The circles and squares correspond to the simulated probability levels, and the line segments are drawn for visual guidance. For $10^{-7} \leq p_F \leq 10^{-2}$, the required number of dynamic analyses grows only slowly: from about 33 to 57 for the estimator associated with m_2, and from about 36 to 81 for the estimator associated with k_2. For $p_F > 10^{-2}$, the computational effort increases markedly as the failure probability grows. These findings suggest that, for this example, the method becomes more efficient as the failure probability decreases. This trend is consistent with the observations reported in [6] for a comparable simulation approach.

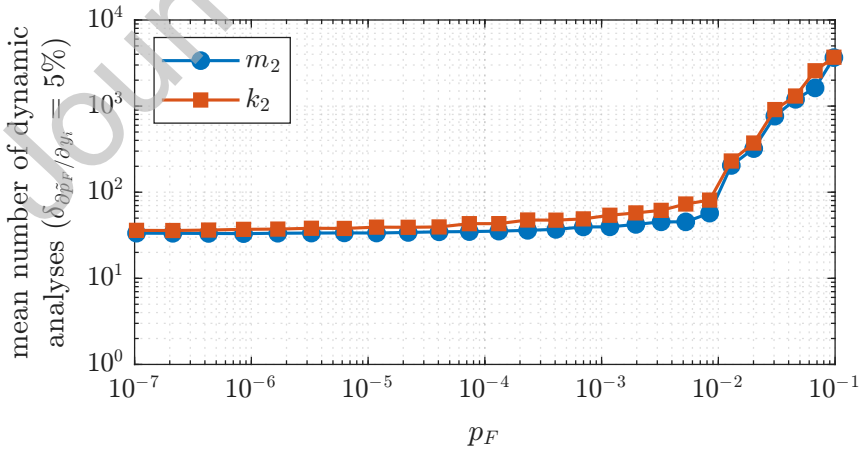

Figure 14: **Example 1:** Mean number of dynamic analyses required by mLS to reach a coefficient of variation of 5% for the sensitivity estimator associated with the parameter k_2, as a function of the first excursion probability p_F.

Estimating the sensitivity with respect to the parameters m_2 and k_2 is crucial for analyzing

vehicle comfort when driving over a road profile. The results shown in Figure 12 indicate that an increase in the car's body mass leads to a higher failure probability of the system. This increase in mass reduces the system's natural frequency, which in turn results in larger displacements due to low-frequency perturbations in the road profile. Moreover, as illustrated in Figure 13, increasing the stiffness k_2 leads to an increase in the system's failure probability. This occurs because a stiffer suspension makes the car react more to irregularities in the road, which increases the displacements and, as a result, the failure probability of the system. From an engineering perspective, the sensitivity estimates provided by the analysis offer guidance at the design stage for tuning the sprung mass and suspension stiffness in order to satisfy comfort and serviceability requirements.

6.3. Example 2: 16-story reinforced concrete building

The second example corresponds to a 3D finite element model of a 16-story reinforced concrete (RC) building, involving 29466 degrees of freedom. This model is based on the example presented in [37] and is illustrated in Figure 16. Each typical floor of the building includes columns and beams, modeled as frame elements, as well as slabs, external walls, and a wall core, modeled as shell elements, as shown in Figure 16a. The frames are represented by black lines; the slabs by light gray surfaces; the external wall by pale yellow surfaces; and the RC shear wall core by light blue surfaces. To highlight the most relevant aspects of the problem, the extrusion of the structural elements has been intentionally omitted in Figure 16. The Young's modulus for the reinforced concrete is taken as $E = 2.5 \times 10^{10}$ N/m^2. The floor height is 3.40 m at the first level and 3.24 m from the second to the sixteenth levels. The slabs and shear walls have thicknesses of 18 cm and 40 cm, respectively. Moreover, the structure is evaluated for serviceability purposes, assuming linear elastic behavior. The first 100 modes are retained for the dynamic analysis to ensure an accurate representation of the response. Extending the scope demonstrated in the previous example, the proposed method can also be applied to a case with proportional damping. In this case, 5% classical damping is considered for all modes.

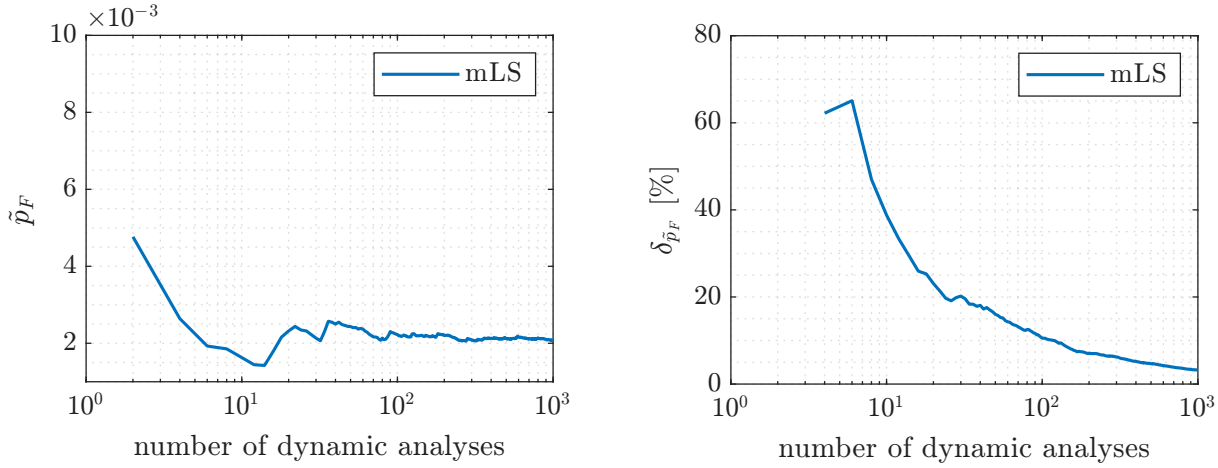

(a) Evolution of the first excursion probability estimator with respect to the number of dynamic analyses.

(b) Coefficient of variation of the first excursion probability estimator with respect to the number of dynamic analyses.

Figure 15: **Example 2:** Evolution of the first excursion probability estimator using multidomain Line Sampling (mLS).

The stochastic ground acceleration acting on the building is modeled as a modulated discrete white noise process, that is passed through a Clough-Penzien filter [54]. It has a spectral intensity of $S = 3 \times 10^{-3}$ m^2/s^3, a time duration of $T = 10$ s, and is discretized into $n_T = 1001$ time steps with a duration of $\Delta t = 0.01$ s. The modulation function $m(t)$ associated with the modulated (hence nonstationary) discrete white-noise input is given by:

$$m(t) = \begin{cases} (t/5)^2 & 0 \leqslant t \leqslant 5[\text{ s}] \\ 1 & 5 < t \leqslant 6[\text{ s}] \\ e^{-(t-6)^2} & t > 6[\text{ s}] \end{cases} . \tag{59}$$

The Clough-Penzien filter is characterized by natural circular frequencies $\omega_{g,1} = 15.6$ rad/s and $\omega_{g,2} = 1.0$ rad/s, and damping ratios $\zeta_{g,1} = 0.6$ and $\zeta_{g,2} = 0.9$. The Karhunen-Loève representation uses the same number of terms as time instants, with $n_{KL} = 1001$, since the focus of this example is to demonstrate the performance of the proposed sensitivity analysis rather than to investigate the effect of the truncation order of the expansion on the results. In addition, the structure is assumed to start from rest.

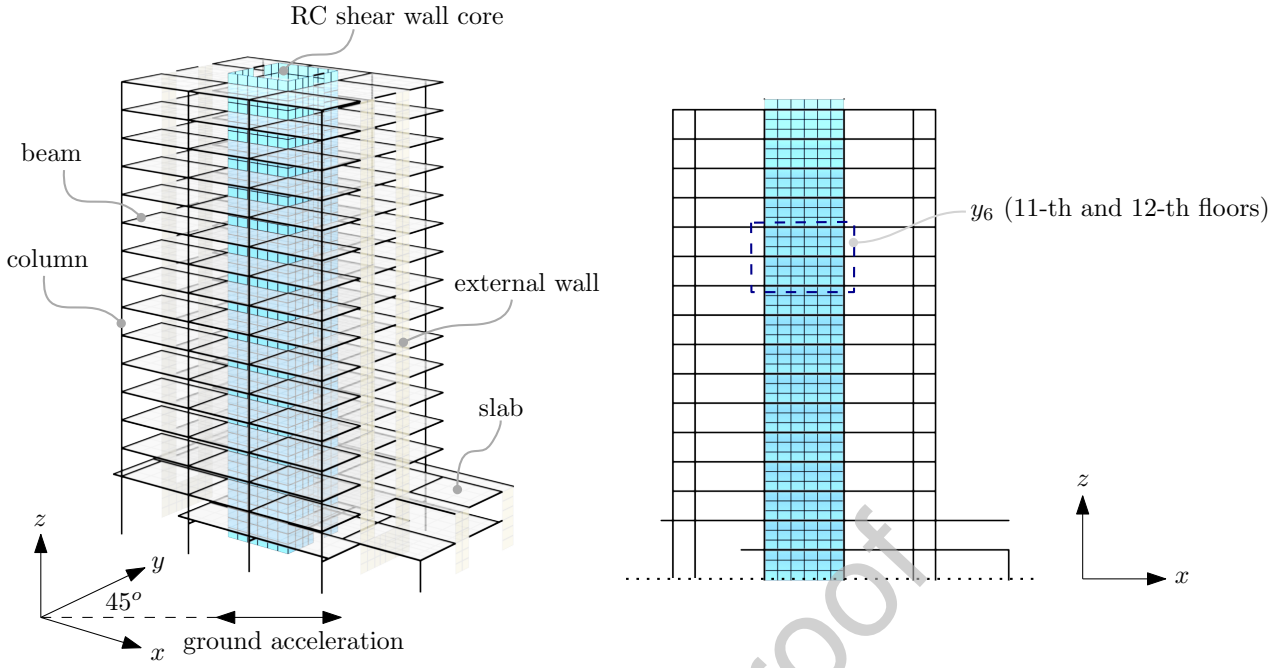

(a) Perspective view. (b) Lateral view.

Figure 16: **Example 2:** 16-story reinforced concrete building model.

The responses of interest correspond to the interstory drifts of the sixteen floors of the building in both the x and y directions, measured from the geometrical center of each floor during the application of the stochastic loading. Therefore, there are a total of $n_\eta = 32$ responses of interest. The threshold limit is set to 0.2% of the floor height, which corresponds to $b_{1-2} = 0.0068$ m for the first floor and $b_{3-32} = 0.0065$ m for the remaining levels. This criterion aligns well with serviceability design purposes. The first excursion probability is estimated using mLS and involves a large number of elementary failure domains ($n_\eta n_{KL} = 32 \times 1001 = 32032$), and the evolution of the corresponding estimator with respect to the number of dynamic analyses is shown in Figure 15a, resulting in $\tilde{p}_F = 2.1 \times 10^{-3}$. Figure 15b presents the evolution of the coefficient of variation of the probability estimate. Although this coefficient of variation is not as small as that observed in the previous example, its decreasing trend is remarkably stable. Indeed, with only about 100 simulation runs, it is possible to estimate a relatively small failure probability with a coefficient of variation of about 10%.

The objective is to estimate the sensitivity of the first excursion probability with respect to the vector $\boldsymbol{y} = [y_1, \ldots, y_8]^T$, where each component y_q represents the thickness of the RC shear wall core at the $(2q-1)$-th and $(2q)$-th floors. This is illustrated in Figure 16b, where, for instance, the parameter y_6 corresponds to the thickness of the RC core walls on the 11th and 12th floors.

The information offered by the sought sensitivities has a very insightful impact in the context of decision making, for instance, reliability-based design [33, 27].

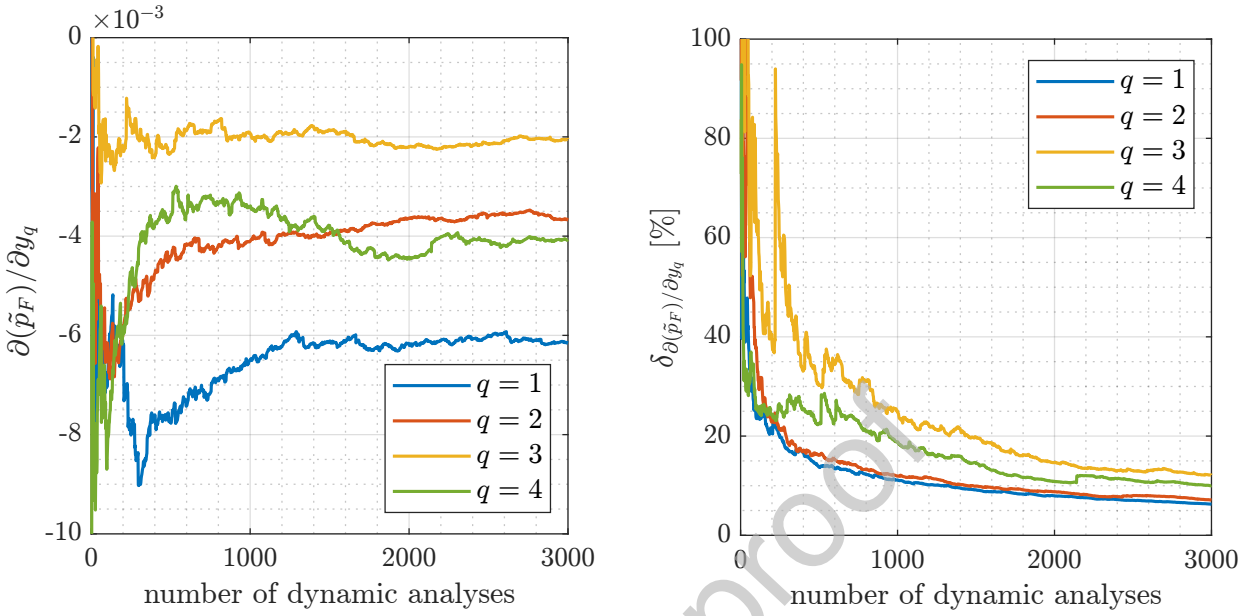

(a) Evolution of the sensitivity estimator with respect to the number of dynamic analyses.

(b) Coefficient of variation of the sensitivity estimator with respect to the number of dynamic analyses.

Figure 17: **Example 2:** Sensitivity results associated with $y_q, q = [1, 2, 3, 4]$ using multidomain Line Sampling (mLS).

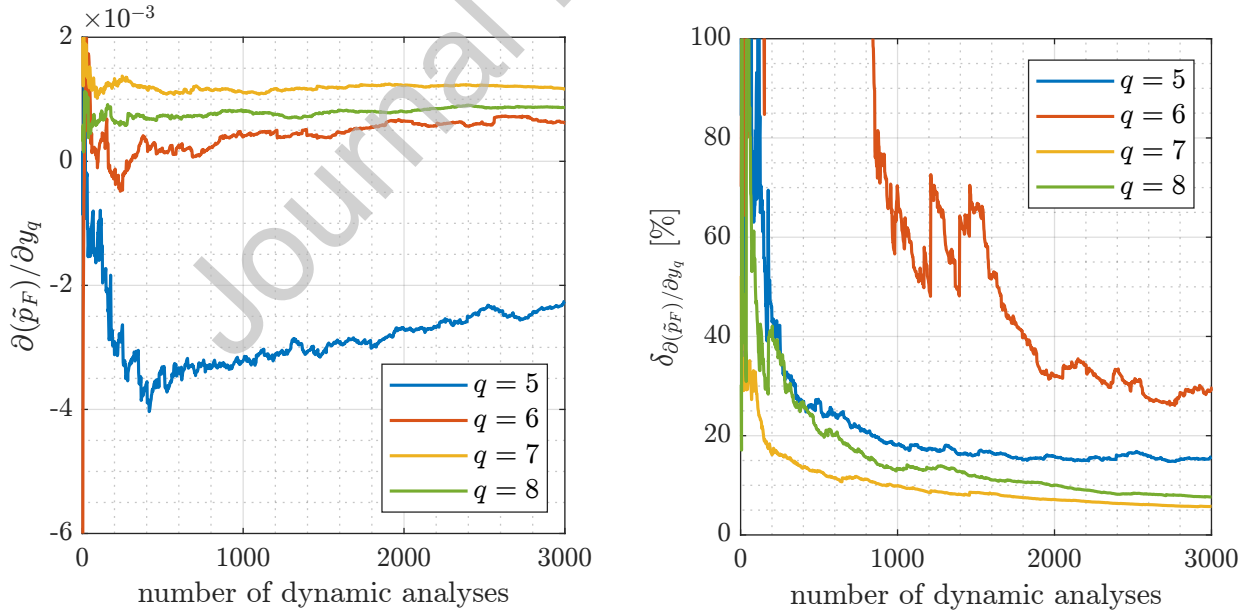

(a) Evolution of the sensitivity estimator with respect to the number of dynamic analyses.

(b) Coefficient of variation of the sensitivity estimator with respect to the number of dynamic analyses.

Figure 18: **Example 2:** Sensitivity results associated with $y_q, q = [5, 6, 7, 8]$ using multidomain Line Sampling (mLS).

The sensitivities were estimated using mLS and the results with respect to parameters $y_q, q = 1, \ldots, 4$ are shown in Figures 17, while the results with respect to the parameters y_q, $q = 5, \ldots, 8$ are illustrated in Figure 18. The evolution of the sensitivities with respect to the number of dynamic analyses, shown in Figure 17a, indicates that increasing y_q, $q = 1, \ldots, 4$, leads to a decrease in the failure probability of the system. In addition, Figure 17b shows that the calculation of the sensitivities is computationally efficient, requiring 250 and 292 dynamic analyses for the estimators associated with y_1 and y_2, respectively, to reach a coefficient of variation of 20%. Moreover, the estimators associated with y_3 and y_4 require 1450 and 978 dynamic analyses, respectively, to achieve the same coefficient of variation. The evolution of the sensitivities with respect to the number of dynamic analyses, shown in Figure 18a, indicates that increasing y_5 leads to a decrease in the failure probability of the system, while increasing the values of y_q, $q = 6, 7, 8$, raises the failure probability. In this case, to reach a coefficient of variation of 20%, the sensitivity related to y_7 requires 148 dynamic analyses, while the one related to y_8 requires 622 dynamic analyses. In addition, to reach a coefficient of variation of 20%, the sensitivity associated with y_5 requires 856 dynamic analyses, while the sensitivity related to y_6 requires 5402 dynamic analyses.

In order to demonstrate the efficiency of mLS compared with existing methods in the literature, such as DIS [8] and DDM [29], the results for the sensitivity related to y_1 are illustrated in Figure 19. It can be observed from Figure 19a that the behavior of the estimator calculated using mLS is notably more stable with fewer dynamic analyses compared to the other methods. This is confirmed in Figure 19b, where approximately 250 dynamic analyses are required for mLS to reach a coefficient of variation of 20%, while DIS and DDM require a total of 1632 and 1801 dynamic analyses, respectively, to achieve the same coefficient of variation. The observed differences between the estimates at lower numbers of dynamic analyses reflect statistical fluctuations and are not indicative of bias. All estimators are theoretically unbiased, and the estimates converge to the true values as the number of dynamic analyses increases. In addition, the speed-up factor $\boldsymbol{S}_u$ was calculated to evaluate the efficiency of mLS in comparison to DIS and DDM for the sensitivity calculation with respect to all design parameters. The corresponding results are presented in Tables 4 and 5. It is worth noting that mLS outperforms DDM in the calculation of all sensitivities, with the lowest speed-up value being 1.05 for the sensitivity related to y_6, and the highest being 30.86 for the sensitivity related to y_7. When compared with DIS, mLS outperforms in the calculation of sensitivities for five out of the eight parameters, with speed-up values

ranging from 1.97 to 7.62. The remaining sensitivities calculated using mLS slightly underperform compared to DIS, with values between 0.57 and 0.94. In general, mLS demonstrates a reduction in the computational effort for all cases, compared with the other methods that behave better for specific cases of sensitivities. This is further supported by the speed-up based on the mean number of dynamic analyses, which is 1.58 when comparing against DIS and 3.36 when comparing against DDM.

In this example, the results are reported in Tables 4 and 5 for a target coefficient of variation of 20% for the sensitivity estimates. This choice represents a trade-off between accuracy and computational cost in the context of a large-scale finite element model, where each dynamic analysis is numerically expensive. For preliminary design studies, a 20% coefficient of variation is typically sufficient, as the sign and relative magnitude of the sensitivities already provide meaningful insight into the influence of the different parameters on the failure probability. It should be emphasized that this target does not represent a limitation of the proposed method: as demonstrated in Example 1, significantly smaller target coefficients of variation (e.g., 5% or even lower) can be attained at increased computational cost.

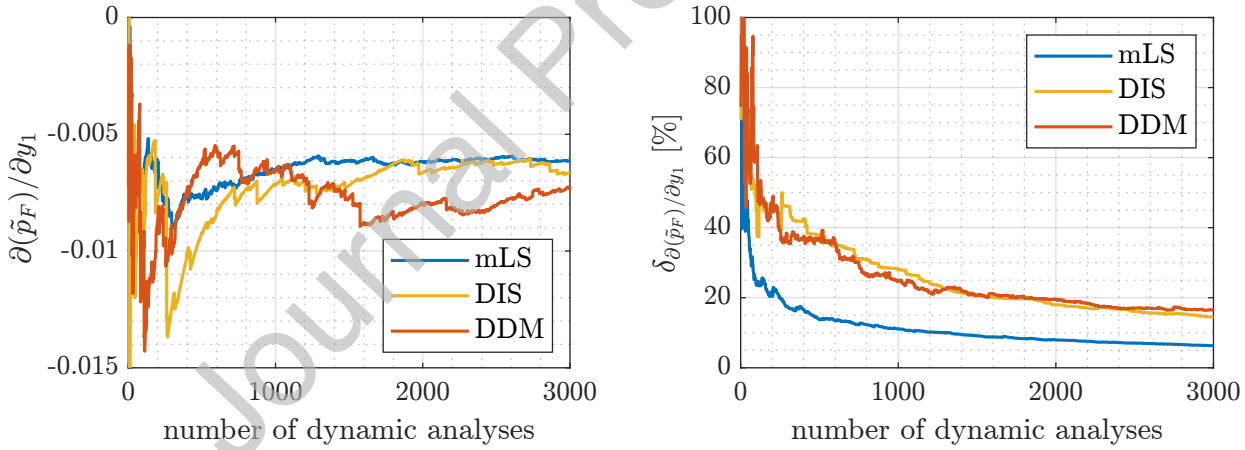

(a) Evolution of the sensitivity estimator with respect to the number of dynamic analyses.

(b) Coefficient of variation of the sensitivity estimator with respect to the number of dynamic analyses.

Figure 19: **Example 2:** Comparison of sensitivity results associated with y_1 using Directional Importance Sampling (DIS), the Domain Decomposition Method (DDM), and multidomain Line Sampling (mLS).

Method	$\partial\tilde{p}_F/\partial y_1$	$\mathrm{N}^{(1)}$	$\partial\tilde{p}_F/\partial y_2$	$\mathrm{N}^{(2)}$	$\partial\tilde{p}_F/\partial y_3$	$\mathrm{N}^{(3)}$	$\partial\tilde{p}_F/\partial y_4$	$\mathrm{N}^{(4)}$
mLS	-8.0×10^{-3}	250	-5.1×10^{-3}	292	-1.9×10^{-3}	1450	-3.4×10^{-3}	948
DIS	-6.8×10^{-3}	1632	-3.8×10^{-3}	1336	-2.5×10^{-3}	823	-3.0×10^{-3}	708
DDM	-8.6×10^{-3}	1801	-3.9×10^{-3}	3341	-2.1×10^{-3}	6720	-3.8×10^{-3}	2607
$\boldsymbol{S}_u$ (mLS vs DIS)	**6.53**		**4.58**		**0.57**		**0.75**	
$\boldsymbol{S}_u$ (mLS vs DDM)	**7.20**		**11.44**		**4.63**		**2.75**	

Table 4: **Example 2:** Sensitivity estimates for y_q, $q = 1, \ldots, 4$, number of dynamic analyses ($\mathrm{N}^{(q)}$), and speed-up ($\boldsymbol{S}_u$) of mLS versus other methods, for a target coefficient of variation of 20%.

Method	$\partial\tilde{p}_F/\partial y_5$	$\mathrm{N}^{(5)}$	$\partial\tilde{p}_F/\partial y_6$	$\mathrm{N}^{(6)}$	$\partial\tilde{p}_F/\partial y_7$	$\mathrm{N}^{(7)}$	$\partial\tilde{p}_F/\partial y_8$	$\mathrm{N}^{(8)}$	$\mathbf{N}_{\mathrm{mean}}$
mLS	-3.3×10^{-3}	856	6.3×10^{-4}	5402	1.3×10^{-3}	148	7.1×10^{-4}	622	**1246.00**
DIS	-2.8×10^{-3}	1684	6.7×10^{-4}	5059	2.0×10^{-3}	1128	7.4×10^{-4}	3392	**1970.25**
DDM	-2.3×10^{-3}	5660	1.0×10^{-3}	5685	1.1×10^{-3}	4568	1.1×10^{-3}	3102	**4185.50**
$\boldsymbol{S}_u$ (mLS vs DIS)	**1.97**		**0.94**		**7.62**		**5.45**		**1.58**
$\boldsymbol{S}_u$ (mLS vs DDM)	**6.61**		**1.05**		**30.86**		**4.99**		**3.36**

Table 5: **Example 2:** Sensitivity estimates for y_q, $q = 5, \ldots, 8$, number of dynamic analyses ($\mathrm{N}^{(q)}$), and speed-up ($\boldsymbol{S}_u$) of mLS versus other methods, for a target coefficient of variation of 20%.

The variation in the number of dynamic analyses required to estimate the different sensitivities, as especially seen in Table 5, is mainly due to the effect of each parameter on the geometry of the elementary failure domains. This is reflected in how the distances $c^j_{[r]}$ change along an exploration line l_j when varying a specific parameter. Parameters that induce stronger and more global modifications in the system response generate larger changes in the crossing distances. In contrast, parameters whose influence is weaker for the entire system, or more localized, lead to smaller sensitivity magnitudes. In both cases, the variance of the estimator depends on how much these induced changes vary from sample to sample: if the impact on the crossing distances remains relatively stable across the exploration lines, the estimator variance is reduced; otherwise, larger sample to sample fluctuations lead to an increase in variance. The different order of magnitude and convergence patterns observed for the sensitivities associated with the parameters y_q in Figures 17 and 18 are a direct manifestation of this same effect.

From a physical point of view, the negative sensitivities with respect to y_q, $q = 1, \ldots, 5$, indicate that increasing the thickness of the walls associated with these design parameters helps reduce the maximum displacements of the building and, consequently, the failure probability. On the

other hand, the positive sensitivities related to y_q, $q = 6, \ldots, 8$, which indicate an increase in the thickness of the walls of the upper floors (from the 11th to the 16th floor), generate a rigid-body effect at the upper part of the building, causing an increase in the maximum displacement and, consequently, in the failure probability of the system. It is important to note that, in magnitude, the positive sensitivities are smaller than the negative ones, which implies that changing the parameters y_q, $q = 1, \ldots, 5$, has a greater effect on the failure probability. The sensitivity estimates provide useful guidance for improving the building's design, especially in early decision-making stages, by identifying the structural parameters that most strongly influence the system reliability.

7. Conclusions and outlook

This work applies multidomain Line Sampling (mLS) to estimate the sensitivity of the first excursion probability in linear systems with non-proportional damping under stochastic Gaussian loading. Sensitivities are computed as partial derivatives of the first excursion probability, incorporating derivatives of the system's spectral properties, eigenvalues, and eigenvectors.

The sensitivities are computed using mLS, which requires fewer dynamic analyses, offering improved efficiency and stability compared to Domain Decomposition Method (DDM) and Directional Importance Sampling (DIS). A key advantage of mLS over DIS lies in its failure domain exploration approach: each exploration line in mLS provides information on the derivative of individual elementary failure domains, while DIS, along a single direction, offers information only on the derivative of the union of all failure domains. Furthermore, a key advantage of mLS over DDM is its perpendicular approach to each elementary failure domain, allowing for more precise sensitivity estimation, whereas DDM follows a directional approach, capturing less information about the sensitivity of the limit state function. Moreover, mLS has demonstrated high efficiency in calculating all sensitivities, whereas DIS and DDM are slightly outperformed in calculating some specific sensitivities.

Potential directions of future research could explore the following:

- The direct application of mLS to the failure probability integral, rather than to the estimation of the effective contribution.
- The effect of the weights as a mass probability function for estimating the effective contributions.

- The estimation of sensitivities with respect to additional model parameters, such as excitation parameters and response thresholds.
- The implementation of the proposed method in reliability-based design optimization (RBDO) problems.
- Extension of the proposed method to systems where the elementary failure domains are weakly non-Gaussian, in line with recent developments on directional sampling methods for non-Gaussian excitation [55]
- An extended formulation of mLS for settings in which, in addition to the stochastic loading, selected structural parameters are also treated as random variables, particularly in cases where this parametric uncertainty is comparable to or dominant over the excitation uncertainty.

The above-mentioned issues are currently being investigated by the authors.

8. Acknowledgments

The author Matthias Faes is an Associate Editor of this journal. In accordance with policy, Matthias Faes was blinded to the entire peer review process. Part of the research was funded by the State Key Laboratory of Disaster Reduction in Civil Engineering, Tongji University under project number SLDRCE24-02. In addition, the financial support from ANID (National Agency for Research and Development, Chile) under its programs FONDECYT (Grant No. 1240013) and FONDECYT de Iniciación (Grant No. 11250068) is also appreciated.

Appendix A. Gradient of the failure probability

The expression in Equation (15) is derived by rewriting the first excursion probability from Equation (10) as:

$$p_F(\boldsymbol{y}) = \int_{\boldsymbol{z}\in\mathbb{R}^{n_{KL}}} H(-g(\boldsymbol{y},\boldsymbol{z}))f_{\boldsymbol{Z}}(\boldsymbol{z})\,d\boldsymbol{z}, \tag{A.1}$$

where $H(\cdot)$ denotes the Heaviside step function. Differentiating Equation (A.1) with respect to a design parameter y_q yields:

$$\frac{\partial p_F(\boldsymbol{y})}{\partial y_q} = -\int_{\boldsymbol{z}\in\mathbb{R}^{n_{KL}}} \delta(-g(\boldsymbol{y},\boldsymbol{z}))\frac{\partial g(\boldsymbol{y},\boldsymbol{z})}{\partial y_q} f_{\boldsymbol{Z}}(\boldsymbol{z})\,d\boldsymbol{z}, \quad q = 1,\ldots,n_Y, \tag{A.2}$$

where $\delta(\cdot)$ denotes the Dirac delta function. Using the identity [56]:

$$\int_{\mathbb{R}^n} f_1(\boldsymbol{x})\delta\left(f_2(\boldsymbol{x})\right)\, d\boldsymbol{x} = \int_{f_2(\boldsymbol{x})=0} \frac{f_1(\boldsymbol{x})}{\|\nabla f_2(\boldsymbol{x})\|}\, d\sigma, \tag{A.3}$$

with $f_1(\boldsymbol{x})$ an arbitrary function, $f_2(\boldsymbol{x})$ a differentiable function with a non-zero gradient at the point where $f_2(\boldsymbol{x}) = 0$, and $d\sigma$ a differential surface element, Equation (A.1) leads to the following expression for the gradient of the failure probability [57]:

$$\frac{\partial p_F(\boldsymbol{y})}{\partial y_q} = -\int_{g(\boldsymbol{y},\boldsymbol{z})=0} \frac{\partial g(\boldsymbol{y},\boldsymbol{z})}{\partial y_q} \frac{1}{\|\nabla_{\boldsymbol{z}} g(\boldsymbol{y},\boldsymbol{z})\|} f_{\boldsymbol{Z}}(\boldsymbol{z})\, dS, \quad q = 1,\ldots,n_Y. \tag{A.4}$$

Appendix B. Brief overview of Line Sampling

Line Sampling [49, 58] aims to estimate the failure probability for performance functions that are weakly or moderately nonlinear [59, 60]. For its deployment, it is assumed that a reliability problem is cast in the standard Gaussian space using an iso-probabilistic transformation. Then, it is necessary to determine the so-called *important direction* $\boldsymbol{\gamma}$, which is a unit Euclidean norm vector originating at the origin and pointing toward the nearest point on the failure domain. This important direction can be determined using different methods, as presented in [49, 61]. Figure B.20 contains a schematic representation of a performance function in a two-dimensional space along the so-called important direction $\boldsymbol{\gamma}$. Due to the rotational invariance of the Gaussian distribution, the Gaussian variable $\boldsymbol{z}$ in the n-dimensional space $\mathbb{R}^n$ can be expressed in terms of a rotated coordinate system as:

$$\boldsymbol{z} = \boldsymbol{R}\boldsymbol{z}^{\perp} + \boldsymbol{\gamma} z^{\parallel}, \tag{B.1}$$

where $\boldsymbol{R}$ is an $n\times(n-1)$ matrix; $\boldsymbol{z}^{\perp}$ is an $(n-1)$-dimensional vector representing the coordinates in the hyperplane orthogonal to $\boldsymbol{\gamma}$; and $z^{\parallel}$ is a scalar representing the coordinate along the direction parallel to $\boldsymbol{\gamma}$. The orthonormal basis of the new coordinate system is defined by the square matrix $[\boldsymbol{R}, \boldsymbol{\gamma}]$. Then, it is possible to demonstrate that $z^{\parallel} = \boldsymbol{\gamma}^T\boldsymbol{z}$ and $\boldsymbol{z}^{\perp} = \boldsymbol{R}^T\boldsymbol{z}$, both of which are associated with standard Gaussian distributions in one dimension and $(n-1)$ dimensions, respectively. It is important to note that, for practical purposes, an explicit form of the matrix $\boldsymbol{R}$ is not required (as explained later in Section 5.1).

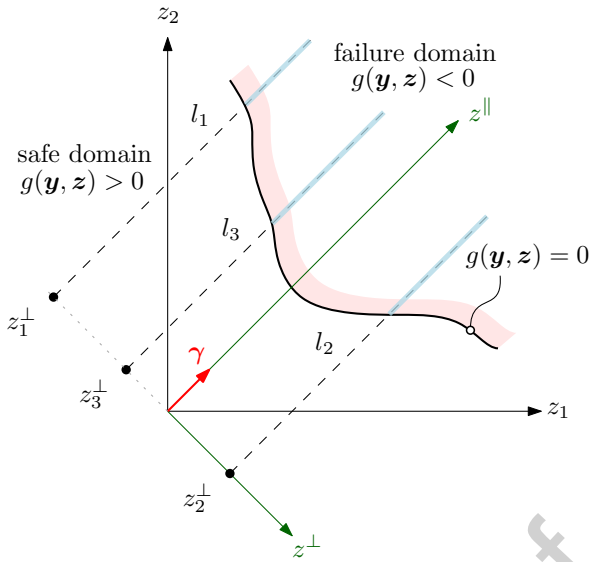

Figure B.20: Schematic representation of Line Sampling technique.

Once the problem is formulated in Gaussian space and the important direction has been determined, the Line Sampling scheme operates by generating $\boldsymbol{z}_j^{\perp}$, $j = 1, \ldots, N$ samples distributed according to a standard Gaussian distribution in $(n-1)$ dimensions, where N denotes the number of samples lying in the hyperplane orthogonal to the important direction $\boldsymbol{\gamma}$ or, equivalently, along the coordinates $\boldsymbol{z}_j^{\perp}$. Then, lines are generated from these samples, denoted as l_j, $j = 1, \ldots, N$, which are parallel to the important direction $\boldsymbol{\gamma}$ and pass through the aforementioned samples $\boldsymbol{z}_j^{\perp}$. Finally, the numerical integration is performed along the one-dimensional lines within the failure domain, and the failure probability is estimated by averaging their contributions. The advantage of employing the rotated coordinate system is that it reduces the multidimensional integration problem to one-dimensional line integrals in standard Gaussian space, which can be evaluated efficiently. The entire process is illustrated in Figure B.20, where the performance function is denoted as $g(\boldsymbol{y}, \boldsymbol{z})$. The generated samples are $\boldsymbol{z}_1^{\perp}$, $\boldsymbol{z}_2^{\perp}$, and $\boldsymbol{z}_3^{\perp}$, and the corresponding lines generated from these samples are denoted as l_1, l_2, and l_3, respectively. The integration over the failure domain is represented by the light blue line. Note that, since this is a bidimensional example, $\boldsymbol{z}^{\perp}$ corresponds to a scalar, whereas in high-dimensional problems, it corresponds to a vector.

Appendix C. Derivative of the effective contribution $\tilde{\boldsymbol{p}}_{s_j}(\boldsymbol{y}, \boldsymbol{z}_j^{\perp})$.

The dependence of the effective contribution on the design vector $\boldsymbol{y}$ is explicitly represented through the integration domain $\Omega(\boldsymbol{y})$, as discussed in Section 4.2 and shown in Equation (30).

This derivative can equivalently be expressed in terms of the indicator function $I_{F_{i,k}}$. Considering the exploration line $l_j(u) = R_{s_j} \boldsymbol{z}_j^{\perp} + \alpha_{s_j} u$, and the integration domain $\Omega_j^{\parallel}(\boldsymbol{y})$ decomposed into $(-\infty, -\beta_{s_j}(\boldsymbol{y})] \cup [\beta_{s_j}(\boldsymbol{y}), +\infty)$, Equation (30) can be written as:

$$\frac{\partial}{\partial y_q} \tilde{p}_{s_j}(\boldsymbol{y}, \boldsymbol{z}_j^{\perp}) = \frac{\partial}{\partial y_q} \left(\int_{-\infty}^{-\beta_{s_j}(\boldsymbol{y})} \frac{I_{F_{s_j}}(l_j(u), \boldsymbol{y})}{\sum_{h=1}^{n_\eta} \sum_{\ell=1}^{n_T} I_{F_{h,\ell}}(l_j(u), \boldsymbol{y})} f_{Z_{s_j}^{\parallel}}(u)\, du + \int_{\beta_{s_j}(\boldsymbol{y})}^{+\infty} \frac{I_{F_{s_j}}(l_j(u), \boldsymbol{y})}{\sum_{h=1}^{n_\eta} \sum_{\ell=1}^{n_T} I_{F_{h,\ell}}(l_j(u), \boldsymbol{y})} f_{Z_{s_j}^{\parallel}}(u)\, du \right), \tag{C.1}$$

where along the exploration line the distribution is standard Gaussian, hence $f_{Z_{s_j}^{\parallel}}(u) = \phi(u)$.

Using the definitions introduced in Section 5 for the crossing distances $c_{[r]}^j(\boldsymbol{y})$, the overlap count $m_{[r]}^j$, and the selector $\kappa_{[r]}^j$, it is possible to write:

$$I_{F_{s_j}}(l_j(u), \boldsymbol{y}) = \sum_{r=1}^{n_S} \kappa_{[r]}^j \Big(H\big(u - c_{[r-1]}^j(\boldsymbol{y})\big) - H\big(u - c_{[r]}^j(\boldsymbol{y})\big) \Big), \tag{C.2}$$

$$\sum_{h=1}^{n_\eta} \sum_{\ell=1}^{n_T} I_{F_{h,\ell}}(l_j(u), \boldsymbol{y}) = \sum_{r=1}^{n_S} m_{[r]}^j \Big(H\big(u - c_{[r-1]}^j(\boldsymbol{y})\big) - H\big(u - c_{[r]}^j(\boldsymbol{y})\big) \Big). \tag{C.3}$$

Thus, the fraction from Equation (C.1) can be expressed as:

$$\frac{I_{F_{s_j}}(l_j(u), \boldsymbol{y})}{\sum_{h=1}^{n_\eta} \sum_{\ell=1}^{n_T} I_{F_{h,\ell}}(l_j(u), \boldsymbol{y})} = \sum_{r=1}^{n_S} \frac{\kappa_{[r]}^j}{m_{[r]}^j} \Big(H\big(u - c_{[r-1]}^j(\boldsymbol{y})\big) - H\big(u - c_{[r]}^j(\boldsymbol{y})\big) \Big). \tag{C.4}$$

The derivative of the Heaviside function with a moving threshold is given by

$$\frac{\partial}{\partial y_q} H\big(u - c_{[r]}^j(\boldsymbol{y})\big) = -\,\delta\big(u - c_{[r]}^j(\boldsymbol{y})\big)\, \frac{\partial c_{[r]}^j(\boldsymbol{y})}{\partial y_q}.$$

Therefore, differentiating Equation (C.4) with respect to the design parameter y_q yields:

$$\frac{\partial}{\partial y_q} \left[\frac{I_{F_{s_j}}(l_j(u), \boldsymbol{y})}{\sum_{h=1}^{n_\eta} \sum_{\ell=1}^{n_T} I_{F_{h,\ell}}(l_j(u), \boldsymbol{y})} \right] = \sum_{r=1}^{n_S} \frac{\kappa_{[r]}^j}{m_{[r]}^j} \Big(\delta\big(u - c_{[r]}^j(\boldsymbol{y})\big)\, \partial_{y_q} c_{[r]}^j(\boldsymbol{y}) - \delta\big(u - c_{[r-1]}^j(\boldsymbol{y})\big)\, \partial_{y_q} c_{[r-1]}^j(\boldsymbol{y}) \Big). \tag{C.5}$$

Finally, using the sifting property [62] $\int_{-\infty}^{\infty} \phi(u)\, \delta(u - c)\, du = \phi(c)$ in Equation (C.1) with

Equation (C.5) gives:

$$\frac{\partial}{\partial y_q}\tilde{p}_{s_j}(\boldsymbol{y},\boldsymbol{z}_j^{\perp}) = \sum_{r=1}^{n_S}\frac{\kappa_{[r]}^j}{m_{[r]}^j}\Big(\phi\Big(c_{[r]}^j(\boldsymbol{y})\Big)\,\partial_{y_q}c_{[r]}^j(\boldsymbol{y}) - \phi\Big(c_{[r-1]}^j(\boldsymbol{y})\Big)\,\partial_{y_q}c_{[r-1]}^j(\boldsymbol{y})\Big), \tag{C.6}$$

which is Equation (52).

Appendix D. Derivative of unit impulse response function

The unit impulse response function in Equation (6) can be rewritten as

$$h_i(t,\boldsymbol{y}) = \sum_{r=1}^{2n_D} A_{r,i}(\boldsymbol{y})B_r(t,\boldsymbol{y}), \tag{D.1}$$

where $i = 1,\ldots,n_\eta$, with

$$A_{r,i}(\boldsymbol{y}) = \frac{\boldsymbol{\gamma}_i^T\boldsymbol{\phi}_r(\boldsymbol{y})\boldsymbol{\phi}_r(\boldsymbol{y})^T\boldsymbol{g}_a(\boldsymbol{y})}{\boldsymbol{\phi}_r(\boldsymbol{y})^T\boldsymbol{M}_a(\boldsymbol{y})\boldsymbol{\phi}_r(\boldsymbol{y})}, \tag{D.2}$$

$$B_r(t,\boldsymbol{y}) = e^{\lambda_r(\boldsymbol{y})t}, \tag{D.3}$$

for $r = 1,\ldots,2n_D$. The partial derivative of $h_i(t,\boldsymbol{y})$ with respect to the design parameter y_q, where $q = 1,\ldots,n_Y$, is given by

$$\frac{\partial h_i(t,\boldsymbol{y})}{\partial y_q} = \sum_{r=1}^{2n_D}\left(\frac{\partial A_{r,i}(\boldsymbol{y})}{\partial y_q}B_r(t,\boldsymbol{y}) + A_{r,i}(\boldsymbol{y})\frac{\partial B_r(t,\boldsymbol{y})}{\partial y_q}\right). \tag{D.4}$$

Defining

$$A_{r,i}^{\{1\}}(\boldsymbol{y}) = \boldsymbol{\gamma}_i^T\boldsymbol{\phi}_r(\boldsymbol{y})\boldsymbol{\phi}_r(\boldsymbol{y})^T\boldsymbol{g}_a(\boldsymbol{y}), \quad A_r^{\{2\}}(\boldsymbol{y}) = \boldsymbol{\phi}_r(\boldsymbol{y})^T\boldsymbol{M}_a(\boldsymbol{y})\boldsymbol{\phi}_r(\boldsymbol{y}),$$

the derivatives in Equation (D.4) are expressed as

$$\frac{\partial A_{r,i}(\boldsymbol{y})}{\partial y_q} = \left(\frac{\partial A_{r,i}^{\{1\}}(\boldsymbol{y})}{\partial y_q}A_r^{\{2\}}(\boldsymbol{y}) - A_{r,i}^{\{1\}}(\boldsymbol{y})\frac{\partial A_r^{\{2\}}(\boldsymbol{y})}{\partial y_q}\right)\frac{1}{\left(A_r^{\{2\}}\right)^2}, \tag{D.5}$$

$$\frac{\partial B_r(t,\boldsymbol{y})}{\partial y_q} = t\,e^{\lambda_r t}\frac{\partial\lambda_r}{\partial y_q}. \tag{D.6}$$

954 Then, the terms in Equation (D.5) are computed as

$$\frac{\partial A_{r,i}^{\{1\}}(\boldsymbol{y})}{\partial y_q} = \boldsymbol{\gamma}_i^T \left(\frac{\partial \boldsymbol{\phi}_r}{\partial y_q} \boldsymbol{\phi}_r^T \boldsymbol{g}_a + \boldsymbol{\phi}_r \left(\frac{\partial \boldsymbol{\phi}_r^T}{\partial y_q} \boldsymbol{g}_a + \boldsymbol{\phi}_r^T \frac{\partial \boldsymbol{g}_a}{\partial y_q} \right) \right), \tag{D.7}$$

$$\frac{\partial A_r^{\{2\}}}{\partial y_q} = \frac{\partial \boldsymbol{\phi}_r^T}{\partial y_q} \boldsymbol{M}_a \boldsymbol{\phi}_r + \boldsymbol{\phi}_r^T \left(\frac{\partial \boldsymbol{M}_a}{\partial y_q} \boldsymbol{\phi}_r + \boldsymbol{M}_a \frac{\partial \boldsymbol{\phi}_r}{\partial y_q} \right). \tag{D.8}$$

955 To evaluate these expressions, the derivatives of the eigenvalue $\lambda_r(\boldsymbol{y})$ and eigenvector $\boldsymbol{\phi}_r(\boldsymbol{y})$
956 with respect to y_q are required. These can be obtained by solving the system proposed in [39],
957 which decouples the sensitivities of each eigenpair:

$$\begin{pmatrix} \boldsymbol{K}_a - \lambda_r \boldsymbol{M}_a & -\boldsymbol{M}_a \boldsymbol{\phi}_r \\ -\boldsymbol{\phi}_r^T \boldsymbol{M}_a & 0 \end{pmatrix} \begin{pmatrix} \dfrac{\partial \boldsymbol{\phi}_r}{\partial y_q} \\ \dfrac{\partial \lambda_r}{\partial y_q} \end{pmatrix} = \begin{pmatrix} -\left(\dfrac{\partial \boldsymbol{K}_a}{\partial y_q} - \lambda_r \dfrac{\partial \boldsymbol{M}_a}{\partial y_q} \right) \boldsymbol{\phi}_r \\ \dfrac{1}{2} \boldsymbol{\phi}_r^T \dfrac{\partial \boldsymbol{M}_a}{\partial y_q} \boldsymbol{\phi}_r \end{pmatrix}. \tag{D.9}$$

958 This formulation assumes mass-normalized mode shapes, i.e., $\boldsymbol{\phi}_r^T(-\boldsymbol{M}_a)\boldsymbol{\phi}_r = 1$, and applies
959 when eigenvalues are distinct. The main advantage of this approach is its independence from the
960 remaining eigenpairs, which simplifies derivative evaluations in modal truncation scenarios [63].

961 Appendix E. Pseudo-code for mLS implementation

962 For ease of numerical implementation, the following pseudo-code summarizes the procedure
963 described in Section5.6, explicitly listing the variables involved at each step together with their
964 governing equations.

Pseudo-code 1: Numerical workflow of the mLS-based sensitivity estimator

Step 1: Representation of Gaussian loading:

$\boldsymbol{p}$; Eq. (1)

Step 2: Definition of structural system:

$\boldsymbol{M}, \boldsymbol{C}, \boldsymbol{K}, \boldsymbol{y}, \boldsymbol{b}$; Eq. (2)

Step 3: Formulation of augmented matrices:

$[\boldsymbol{M}_a], [\boldsymbol{K}_a], \{\boldsymbol{g}_a\}$; Eqs. (3)–(4)

Step 4: Calculation of spectral vectors:

$\boldsymbol{a}_{i,k}$, $\partial_{y_q}\boldsymbol{a}_{i,k}$; Eqs. (6),(57)

Step 5: mLS loop:

for $j = 1$ **to** N **do**

- **(a)** $\boldsymbol{z}_j^{\perp}$, l_j; Sec. 5.1
- **(b)** $c_{i,k}^{\pm,j}$, $v_{i,k}^{\pm,j}$; Eqs. (38)–(42)
- **(c)** $\tilde{\mathcal{C}}_{\text{sort}}^{j}$, $\tilde{\mathcal{V}}_{\text{sort}}^{j}$; Eqs. (41),(43)
- **(d)** λ_N^j, λ_P^j; Eq. (44)
- **(e)** $\partial c_{i,k}^{\pm,j}/\partial y_q$, $\mathcal{D}^j$, $\tilde{\mathcal{D}}_{\text{sort}}^{j}$; Eqs. (53)–(56)
- **(f)** $\boldsymbol{m}^j$, $\boldsymbol{\kappa}^j$; Eqs. (48)–(50)
- **(g)** $\tilde{p}_{s_j}$, $\partial_{y_q}\tilde{p}_{s_j}$; Eqs. (51),(52)

Step 6: Aggregation:

$\tilde{p}_F$, $\partial_{y_q}\tilde{p}_F$; Eqs. (23),(29)

References

[1] T. Soong, M. Grigoriu, Random Vibration of Mechanical and Structural Systems, Prentice Hall, Englewood Cliffs, New Jersey, 1993.

[2] J.-S. Yang, M.-Z. Lyu, J.-B. Chen, J.-Y. Xue, Structural design optimization under stochastic excitations considering first-passage probability constraint based on dimension-reduced probability density evolution equation, Reliability Engineering & System Safety 264 (2025) 111378. doi:https://doi.org/10.1016/j.ress.2025.111378.
URL https://www.sciencedirect.com/science/article/pii/S0951832025005794

[3] D. García, M. Rosales, R. Sampaio, Dynamic behaviour of a timber footbridge with uncertain material properties under a single deterministic walking load, Structural Safety 77 (2019) 10 – 17. doi:https://doi.org/10.1016/j.strusafe.2018.11.001.
URL http://www.sciencedirect.com/science/article/pii/S0167473018301127

[4] M. Huang, C. Chan, W. Lou, Optimal performance-based design of wind sensitive

tall buildings considering uncertainties, Computers & Structures 98-99 (2012) 7–16. doi:10.1016/j.compstruc.2012.01.012.

[5] D. Honfi, A. Mårtensson, S. Thelandersson, Reliability of beams according to eurocodes in serviceability limit state, Engineering Structures 35 (2012) 48–54. doi:10.1016/j.engstruct.2011.11.003.

[6] S. Au, J. Beck, First excursion probabilities for linear systems by very efficient importance sampling, Probabilistic Engineering Mechanics 16 (3) (2001) 193–207.

[7] L. Katafygiotis, S. Cheung, Domain decomposition method for calculating the failure probability of linear dynamic systems subjected to Gaussian stochastic loads, Journal of Engineering Mechanics 132 (5) (2006) 475–486.

[8] M. Misraji, M. Valdebenito, H. Jensen, C. Mayorga, Application of directional importance sampling for estimation of first excursion probabilities of linear structural systems subject to stochastic Gaussian loading, Mechanical Systems and Signal Processing 139 (2020) 106621. doi:https://doi.org/10.1016/j.ymssp.2020.106621.
URL http://www.sciencedirect.com/science/article/pii/S0888327020300078

[9] M. Valdebenito, P. Wei, J. Song, M. Beer, M. Broggi, Failure probability estimation of a class of series systems by multidomain Line Sampling, Reliability Engineering & System Safety 213 (2021) 107673. doi:https://doi.org/10.1016/j.ress.2021.107673.
URL https://www.sciencedirect.com/science/article/pii/S0951832021002118

[10] S. Benfratello, S. Caddemi, G. Muscolino, Gaussian and non-gaussian stochastic sensitivity analysis of discrete structural system, Computers & Structures 78 (1) (2000) 425 – 434. doi:https://doi.org/10.1016/S0045-7949(00)00086-9.
URL http://www.sciencedirect.com/science/article/pii/S0045794900000869

[11] J. Chen, Z. Wan, M. Beer, A global sensitivity index based on Fréchet derivative and its efficient numerical analysis, Probabilistic Engineering Mechanics 62 (2020) 103096. doi:https://doi.org/10.1016/j.probengmech.2020.103096.
URL http://www.sciencedirect.com/science/article/pii/S0266892020300837

[12] T. Hien, M. Kleiber, Stochastic design sensitivity in structural dynamics, International Journal for Numerical Methods in Engineering 32 (6) (1991) 1247–1265. arXiv:https://onlinelibrary.wiley.com/doi/pdf/10.1002/nme.1620320606, doi:https://doi.org/10.1002/nme.1620320606.
URL https://onlinelibrary.wiley.com/doi/abs/10.1002/nme.1620320606

[13] G. Muscolino, R. Santoro, A. Sofi, Explicit reliability sensitivities of linear structures with interval uncertainties under stationary stochastic excitation, Structural Safety 52, Part B (2015) 219 – 232, engineering Analyses with Vague and Imprecise Information. doi:http://dx.doi.org/10.1016/j.strusafe.2014.03.001.
URL http://www.sciencedirect.com/science/article/pii/S0167473014000198

[14] A. Suksuwan, S. Spence, Optimization of uncertain structures subject to stochastic wind loads under system-level first excursion constraints: A data-driven approach, Computers & Structures 210 (2018) 58 – 68. doi:https://doi.org/10.1016/j.compstruc.2018.09.001.
URL http://www.sciencedirect.com/science/article/pii/S0045794917314566

[15] P. Bjerager, Probability computation methods in structural and mechanical reliability, in: W. Liu, T. Belytschko (Eds.), Mechanics of Probabilistic and Reliability Analysis, Elme Press International, Lausanne, Switzerland, 1989, pp. 48–67.

[16] Y. Wu, Computational methods for efficient structural reliability and reliability sensitivity analysis, AIAA Journal 32 (8) (1994) 1717–1723.

[17] K. Marti, Differentiation of probability functions: The transformation method, Computers Mathematics with Applications 30 (3-6) (1995) 361–382.

[18] S. Song, Z. Lu, H. Qiao, Subset simulation for structural reliability sensitivity analysis, Reliability Engineering & System Safety 94 (2) (2009) 658–665. doi:10.1016/j.ress.2008.07.006.

[19] I. Papaioannou, K. Breitung, D. Straub, Reliability sensitivity analysis with Monte Carlo methods, in: B. E. G. Deodatis, D. Frangopol (Eds.), 11th International Conference on Structural Safety and Reliability (ICOSSAR), New York, NY, USA, 2013, pp. 5335–5342.

[20] I. Papaioannou, K. Breitung, D. Straub, Reliability sensitivity estimation with sequential importance sampling, Structural Safety 75 (2018) 24 – 34. doi:https://doi.org/10.1016/j.strusafe.2018.05.003.
URL http://www.sciencedirect.com/science/article/pii/S0167473017304459

[21] H. Jensen, F. Mayorga, M. Valdebenito, Reliability sensitivity estimation of nonlinear structural systems under stochastic excitation: A simulation-based approach, Computer Methods in Applied Mechanics and Engineering 289 (2015) 1–23. doi:http://dx.doi.org/10.1016/j.cma.2015.01.012.
URL http://www.sciencedirect.com/science/article/pii/S0045782515000250

[22] H. Jensen, F. Mayorga, C. Papadimitriou, Reliability sensitivity analysis of stochastic finite element models, Computer Methods in Applied Mechanics and Engineering 296 (2015) 327–351. doi:http://dx.doi.org/10.1016/j.cma.2015.08.007.
URL http://www.sciencedirect.com/science/article/pii/S0045782515002613

[23] S. Chakraborty, B. Roy, Reliability based optimum design of tuned mass damper in seismic vibration control of structures with bounded uncertain parameters, Probabilistic Engineering Mechanics 26 (2) (2011) 215–221.

[24] S. Au, Reliability-based design sensitivity by efficient simulation, Computers & Structures 83 (14) (2005) 1048–1061.

[25] J. Ching, Y. Hsieh, Local estimation of failure probability function and its confidence interval with maximum entropy principle, Probabilistic Engineering Mechanics 22 (1) (2007) 39–49.

[26] H. Jensen, M. Valdebenito, G. Schuëller, D. Kusanovic, Reliability-based optimization of stochastic systems using line search, Computer Methods in Applied Mechanics and Engineering 198 (49-52) (2009) 3915–3924.

[27] M. Valdebenito, G. Schuëller, Efficient strategies for reliability-based optimization involving non linear, dynamical structures, Computers & Structures 89 (19-20) (2011) 1797–1811.

[28] M. Valdebenito, H. Jensen, G. Schuëller, F. Caro, Reliability sensitivity estimation of linear systems under stochastic excitation, Computers & Structures 92-93 (2012) 257–268. doi:10.1016/j.compstruc.2011.10.020.

[29] M. A. Misraji, M. A. Valdebenito, M. G. Faes, First excursion probability sensitivity in stochastic linear dynamics by means of domain decomposition method, Mechanical Systems and Signal Processing 235 (2025) 112865. doi:10.1016/j.ymssp.2025.112865.

[30] P. Bjerager, Probability integration by directional simulation, Journal of Engineering Mechanics 114 (8) (1988) 1285–1297.

[31] O. Ditlevsen, P. Bjerager, R. Olesen, A. Hasofer, Directional simulation in Gaussian processes, Probabilistic Engineering Mechanics 3 (4) (1988) 207 – 217. doi:https://doi.org/10.1016/0266-8920(88)90013-6.
URL http://www.sciencedirect.com/science/article/pii/0266892088900136

[32] A. Beck, W. Gomes, R. Lopez, L. Miguel, A comparison between robust and risk-based optimization under uncertainty, Structural and Multidisciplinary Optimization 52 (3) (2015)

479–492. doi:10.1007/s00158-015-1253-9.
URL http://dx.doi.org/10.1007/s00158-015-1253-9

[33] G. Schuëller, H. Jensen, Computational methods in optimization considering uncertainties – An Overview, Computer Methods in Applied Mechanics and Engineering 198 (1) (2008) 2–13. doi:10.1016/j.cma.2008.05.004.

[34] D. Jerez, H. Jensen, M. Valdebenito, M. Misraji, F. Mayorga, M. Beer, On the use of directional importance sampling for reliability-based design and optimum design sensitivity of linear stochastic structures, Probabilistic Engineering Mechanics 70 (2022) 103368. doi:https://doi.org/10.1016/j.probengmech.2022.103368.
URL https://www.sciencedirect.com/science/article/pii/S0266892022001011

[35] H. Jensen, A. Muñoz, C. Papadimitriou, E. Millas, Model-reduction techniques for reliability-based design problems of complex structural systems, Reliability Engineering & System Safety 149 (2016) 204–217. doi:https://doi.org/10.1016/j.ress.2016.01.003.
URL https://www.sciencedirect.com/science/article/pii/S0951832016000120

[36] W.-H. Kang, J. Song, P. Gardoni, Matrix-based system reliability method and applications to bridge networks, Reliability Engineering & System Safety 93 (11) (2008) 1584–1593. doi:https://doi.org/10.1016/j.ress.2008.02.011.
URL https://www.sciencedirect.com/science/article/pii/S0951832008000392

[37] M. Valdebenito, M. Misraji, H. Jensen, C. Mayorga, Sensitivity estimation of first excursion probabilities of linear structures subject to stochastic gaussian loading, Computers & Structures 248 (2021) 106482. doi:https://doi.org/10.1016/j.compstruc.2021.106482.
URL https://www.sciencedirect.com/science/article/pii/S0045794921000043

[38] S. Adhikari, Structural dynamic analysis with generalized damping models, Mechanical engineering and solid mechanics series, ISTE ;, London ;, 2014, includes bibliographical references and index. - Description based on print version record.

[39] I.-W. Lee, G.-H. Jung, An efficient algebraic method for the computation of natural frequency and mode shape sensitivities - part I. distinct natural frequencies, Computers & Structures 62 (3) (1997) 429–435. doi:http://dx.doi.org/10.1016/S0045-7949(96)00206-4.
URL http://www.sciencedirect.com/science/article/pii/S0045794996002064

[40] C. Schenk, G. Schuëller, Uncertainty Assessment of Large Finite Element Systems, Springer-Verlag, Berlin/Heidelberg/New York, 2005.

[41] G. Stefanou, The stochastic finite element method: Past, present and future, Computer Methods in Applied Mechanics and Engineering 198 (9-12) (2009) 1031–1051.

[42] A. Chopra, Dynamics of structures: theory and applications to earthquake engineering, Prentice Hall, 1995.

[43] F. Y. Cheng, Matrix Analysis of Structural Dynamics, CRC, 2000.

[44] H. Jensen, M. Valdebenito, Reliability analysis of linear dynamical systems using approximate representations of performance functions, Structural Safety 29 (3) (2007) 222–237.

[45] W. Gautschi, Numerical Analysis, 2nd Edition, Birkhäuser Boston, 2012. doi:10.1007/978-0-8176-8259-0.

[46] G. Schuëller, H. Pradlwarter, Benchmark study on reliability estimation in higher dimensions of structural systems – An overview, Structural Safety 29 (2007) 167–182.

[47] A. Der Kiureghian, The geometry of random vibrations and solutions by FORM and SORM, Probabilistic Engineering Mechanics 15 (1) (2000) 81–90.

[48] K. Breitung, The return of the design points, Reliability Engineering & System Safety 247 (2024) 110103. doi:https://doi.org/10.1016/j.ress.2024.110103.

URL https://www.sciencedirect.com/science/article/pii/S0951832024001777

[49] P. Koutsourelakis, H. Pradlwarter, G. Schuëller, Reliability of structures in high dimensions, part I: Algorithms and applications, Probabilistic Engineering Mechanics 19 (4) (2004) 409–417.

[50] Z. Lu, S. Song, Z. Yue, J. Wang, Reliability sensitivity method by line sampling, Structural Safety 30 (6) (2008) 517–532. doi:10.1016/j.strusafe.2007.10.001.

[51] E. Zio, The Monte Carlo Simulation Method for System Reliability and Risk Analysis, Springer London, 2013.

[52] H. Flanders, Differentiation under the integral sign, The American Mathematical Monthly 80 (6) (1973) 615–627.
URL http://www.jstor.org/stable/2319163

[53] X. Yuan, S. Liu, M. Valdebenito, M. Faes, D. Jerez, H. Jensen, M. Beer, Decoupled reliability-based optimization using Markov chain Monte Carlo in augmented space, Advances in Engineering Software 157-158 (2021) 103020. doi:https://doi.org/10.1016/j.advengsoft.2021.103020.
URL https://www.sciencedirect.com/science/article/pii/S0965997821000491

[54] A. Zerva, Spatial Variation of Seismic Ground Motions – Modeling and Engineering Applications, CRC Press, 2009.

[55] X.-Y. Zhang, M. A. Misraji, M. A. Valdebenito, M. G. Faes, Directional importance sampling for dynamic reliability of linear structures under non-gaussian white noise excitation, Mechanical Systems and Signal Processing 224 (2025) 112182. doi:https://doi.org/10.1016/j.ymssp.2024.112182.
URL https://www.sciencedirect.com/science/article/pii/S0888327024010811

[56] L. Zhang, Dirac Delta function of matrix argument, International Journal of Theoretical Physics.
URL https://doi.org/10.1007/s10773-020-04598-8

[57] I. Elishakoff, Probabilistic Theory of Structures, Dover Publications, New York, 1999.

[58] G. Schuëller, H. Pradlwarter, P. Koutsourelakis, A critical appraisal of reliability estimation procedures for high dimensions, Probabilistic Engineering Mechanics 19 (4) (2004) 463–474.

[59] M. F. Pellissetti, G. I. Schuëller, H. J. Pradlwarter, A. Calvi, S. Fransen, M. Klein, Reliability analysis of spacecraft structures under static and dynamic loading, Computers & Structures 84 (21) (2006) 1313–1325.

[60] M. Valdebenito, H. Jensen, H. Hernández, L. Mehrez, Sensitivity estimation of failure probability applying line sampling, Reliability Engineering & System Safety 171 (2018) 99–111. doi:https://doi.org/10.1016/j.ress.2017.11.010.
URL https://www.sciencedirect.com/science/article/pii/S0951832017308025

[61] M. de Angelis, E. Patelli, M. Beer, Advanced Line Sampling for efficient robust reliability analysis, Structural Safety 52, Part B (2015) 170–182. doi:http://dx.doi.org/10.1016/j.strusafe.2014.10.002.
URL http://www.sciencedirect.com/science/article/pii/S0167473014000927

[62] R. N. Bracewell, Fourier transform and its applications, 3rd Edition, McGraw Hill Higher Education, Maidenhead, England, 1999.

[63] R. Nelson, Simplified calculation of eigenvector derivatives, AIAA Journal 14 (9) (1976) 1201–1205.

Declaration of interests

The authors declare that they have no known competing financial interests or personal relationships that could have appeared to influence the work reported in this paper.